Volume 56
Number 59
28 July 2020
Pages 8153–8318

ChemComm

Chemical Communications

rsc.li/chemcomm

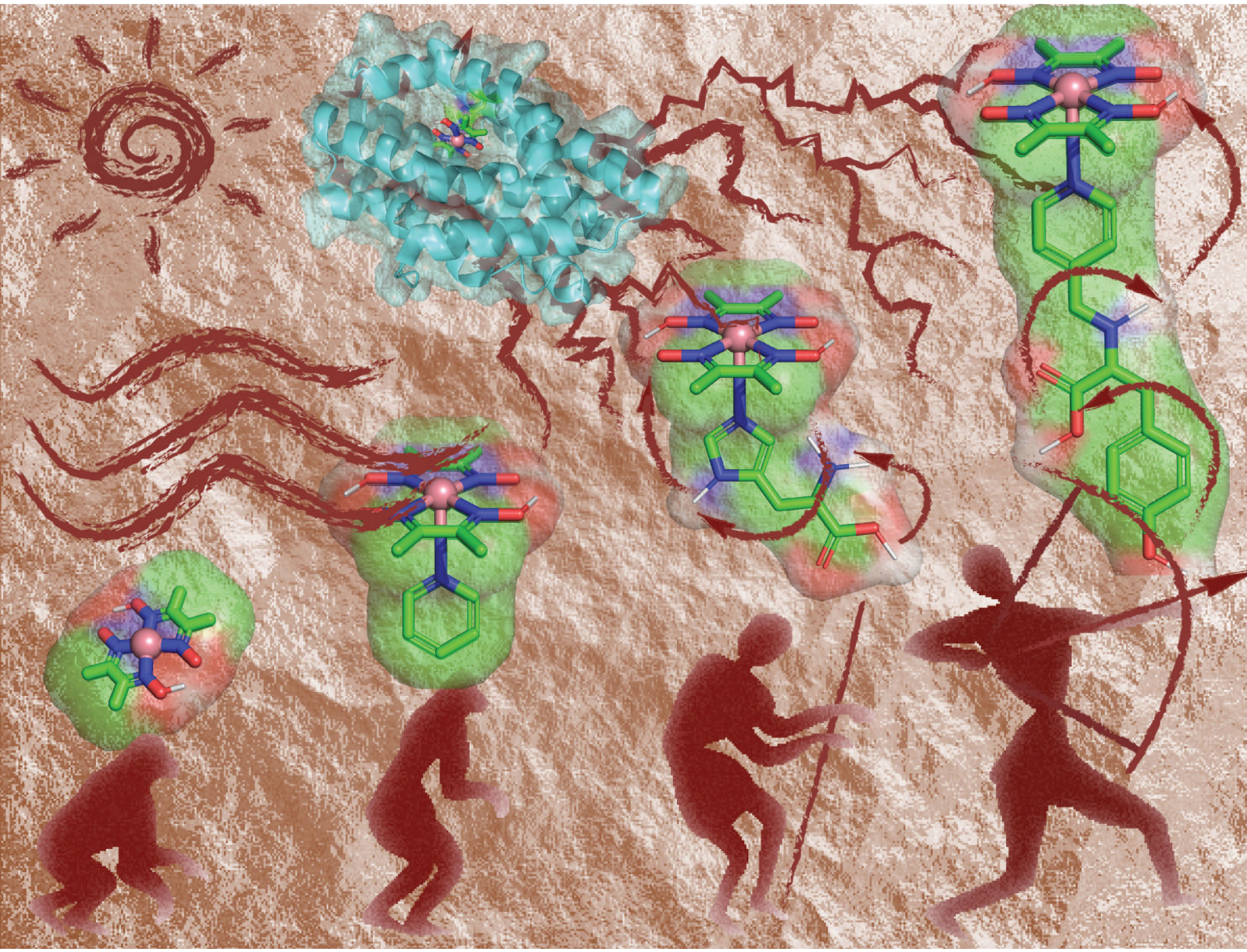

ISSN 1359-7345

ROYAL SOCIETY OF CHEMISTRY

FEATURE ARTICLE

Arnab Dutta *et al.*

The odyssey of cobaloximes for catalytic H_2 production and their recent revival with enzyme-inspired design

ChemComm

FEATURE ARTICLE

View Article Online
View Journal | View Issue

Check for updates

Cite this: *Chem. Commun.*, 2020, **56**, 8166

The odyssey of cobaloximes for catalytic H_2 production and their recent revival with enzyme-inspired design

Dependu Dolui [a] Shikha Khandelwal, [a] Piyali Majumder [b] and Arnab Dutta *[c]

Received 29th April 2020,
Accepted 5th June 2020

DOI: 10.1039/d0cc03103h

rsc.li/chemcomm

Cobaloxime complexes gained attention for their intrinsic ability of catalytic H_2 production despite their initial emergence as a vitamin B12 model. The simple, robust, and synthetically manoeuvrable cobaloxime core represents a model catalyst molecule for the investigation of optimal conditions for both photo- and electrocatalytic H_2 production catalytic assemblies. Cobaloxime is one of the rare catalysts that finds equal applications in the analysis of homogeneous and heterogeneous catalytic conditions. However, the poor aqueous solubility and long-term instability of cobaloximes have severely impeded their growth. Lately, interest in the cobaloxime-based catalysts has been resuscitated with the rational use of extended enzymatic features. This unique enzyme-inspired catalyst design strategy has instigated the formation of a new genre of cobaloxime molecules that exhibit enhanced photo- and electrocatalytic H_2 evolution with improved aqueous and air stability.

Published on 05 June 2020. Downloaded on 1/24/2026 11:49:52 AM.

Introduction

The structural elucidation of vitamin B12 sprung a surprise in the bioinorganic community with the presence of a rare organometallic cobalt–carbon bond in biology.[1–3] Vitamin B12 performs an array of metabolically vital chemical reactions such as methyl transfer, dehalogenation, and isomerization. Hence, the basic structure of vitamin B12 soon became the source of inspiration for developing several biomimetic model complexes

[a] *Chemistry Discipline, Indian Institute of Technology Gandhinagar, Palaj 382355, India*
[b] *Biological Engineering Discipline, Indian Institute of Technology Gandhinagar, Palaj 382355, India*
[c] *Chemistry Department, Indian Institute of Technology Bombay, Powai 400076, India. E-mail: arnabdutta@chem.iitb.ac.in*

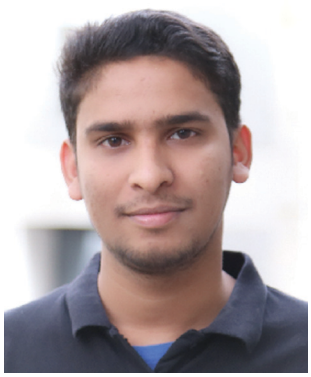

Dependu Dolui

Dependu Dolui obtained his Master's degree with a specialization in Inorganic Chemistry from the Central University of Punjab (CUPB) (2017). After receiving the DST-Inspire Fellowship for Doctoral Research in India, he joined the bioinorganic research group of Dr Arnab Dutta at the Indian Institute of Technology, Gandhinagar (IITGN). His major research interests focus on designing bio-inspired molecular catalysts for energy-relevant small molecule activation and chemical transformation. In his free time, he loves to travel.

Shikha Khandelwal

Shikha Khandelwal received her Master's degree in Chemistry from the School of Chemical Sciences, DAVV, Indore, India. She joined IIT Gandhinagar to pursue a PhD in inorganic chemistry under the supervision of Dr Arnab Dutta. Her research focuses on the development of a cobalt-based synthetic catalyst inspired by natural enzymes for the hydrogen evolution reaction (HER).

This journal is © The Royal Society of Chemistry 2020

Published on 05 June 2020. Downloaded on 1/24/2026 11:49:52 AM.

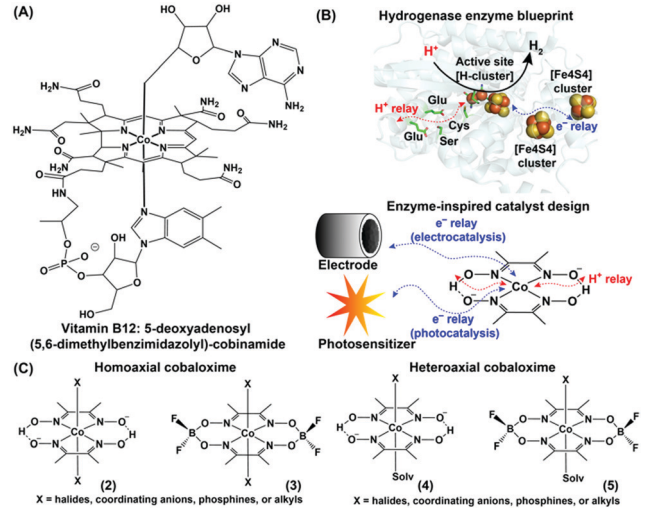

Fig. 1 (A) Chemical structures of the vitamin B12 core (cobinamide). (B) Inclusion of the H^+ relay and electron channel around the metal active site in the hydrogenase enzyme (PDB: 1HFE) and synthetic cobaloxime. The electron for the synthetic cobaloxime is transported from the electrode (electrocatalysis) or excited photosensitizer (photocatalysis). (C) Comparative structures of homo- and hetero-axial cobaloximes.

for executing versatile industry-relevant chemical reactions, including alkene coupling, ring-opening metathesis, hydrogenation, and rearrangement.[4] A stable organometallic cobalt complex, 5-deoxyadenosyl(5,6-dimethylbenzimidazolyl)-cobinamide (**(1)**, Fig. 1A), resides in the core of vitamin B12, where the equatorial corrin ring plays a crucial role in tuning its reactivity.[5] The requirement of such a bulky and synthetically challenging tetradentate corrin ring can be avoided by innovative substitution with two molecules of bidentate dimethyl glyoximes while retaining the versatile edge of a Co–N_4 square planar core structure.[6,7] Schrauzer and Kohnle prepared one of the first examples of such square planar cobalt dimethylglyoxime complexes, where the axial coordination sites were occupied by cyanide and pyridine groups.[8] Following up on this work, Wagner and Bernhauer replaced the axial cyanide group with a Grignard reagent to generate an air-stable cobalt-alkyl derivative, imitating the vitamin B12 coenzyme core.[9] Later, the term "*cobaloxime*" was coined to describe the cobalt dimethylglyoxime [$Co(DH)_2$] moiety. The unique structure of these vitamin B12-inspired cobaloximes has instigated a series of attempts to probe their activity even as a functional model for the hydrogenase enzyme. The excellent reactivity of hydrogenases for H_2 production ($2H^+ + 2e^- \leftrightharpoons H_2$) is attributed to the synchronized conglomeration of a redox-active metal cofactor, electron-transporting [FeS] cluster proteins, and proton-relaying polar amino acid side-chains. Among these, the redox-active metal core and closely lying polar functionalities (oximes) are already present in cobaloximes. Hence, an appropriate electron supplement (either from a photo- or potential-driven source) can activate the cobaloximes for the catalytic hydrogen evolution reaction (HER) (Fig. 1B).

This first proof of this "enzyme-inspired catalyst design" hypothesis was provided by Ziessel and co-workers, who observed photocatalytic H_2 production by cobaloximes in the presence of $[Ru(bpy)_3]^{2+}$ and an organic amine as the photosensitizer and electron donor, respectively.[10] Here, the Co(II) centre of cobaloximes readily coverts to Co(I) following the reductive quenching of photo-excited $[Ru(bpy)_3]^{2+}$. Next, the subsequent protonation generates a highly reactive Co(III)-hydride intermediate, which ultimately decomposes to display H_2 production. The intrinsic O_2 tolerance of cobaloximes allowed the occurrence of this catalytic H_2 production even in aerobic conditions. Despite exhibiting such unique catalytic HER activity, cobaloximes failed to achieve prominence as HER

Piyali Majumder

Piyali Majumder completed her Bachelor's degree in Biochemistry from Presidency College (2010), followed by a Master's degree in Biotechnology from the University of Calcutta (CU) (2012). Then, she joined the Saha Institute of Nuclear Physics (SINP) under the guidance of Dr Debashis Mukhopadhyay. After her PhD, she was awarded a National Post-doctorate Fellowship to work with Dr Bhaskar Datta at the Indian Institute of Technology Gandhinagar (IITGN). She specializes in the biochemistry of neurodegenerative diseases and metalloenzyme activity.

Arnab Dutta

The intricate framework of natural metalloenzymes has always fascinated Arnab Dutta from the beginning. He had an opportunity to study those structural marvels of biology during his PhD with Dr Anne Jones, where he developed metallopetide-based candid models of hydrogenase (Arizona State University, 2012). In the next phase of his career, he mastered the finer details of enzyme-mimicry with Dr Wendy Shaw. This time, he generated versatile molecular catalysts, boasting minimal but essential enzymatic traits in their periphery (Pacific Northwest National Laboratory, 2015). As an independent researcher, he is trying to develop sustainable and all-weather ready catalysts that can boost the use of renewable energy. His quest to bring life into poorly active catalysts with the Midas touch of enzyme-derived features continues at IIT Bombay.

Published on 05 June 2020. Downloaded on 1/24/2026 11:49:52 AM.

catalysts due to their long-term instability.[11,12] In biology, the axial ligands are believed to bring the stability for the cobalt-core in vitamin B12.[13] Following this cue, several ligands (halides, coordinating mono-anions, phosphines, alkyls, and even coordinating solvent molecules) were screened in the pursuit of stable cobaloxime [$XCo(DH)_2B$] motifs. The internal hydrogen-bonding network of oxime (–N–OH···O^-–N–) groups were further difluoroborylated (BF_2) to generate derivatives of cobaloximes [$XCo(DBF_2)_2B$], while the identity of the axial ligands was utilized to classify them into homo- or hetero-axial cobaloximes (**(2–5)**, Fig. 1C).[14] Introduction of these electron-withdrawing difluoroboryl (BF_2)-functionality shrinks the energy barrier for catalytically vital cobalt reduction steps.[15] Espenson *et al.* was able to utilize this thermodynamic advantage, and reported on the chemical H_2 production from hydrochloric acid by [$XCo(DBF_2)_2B$] in the presence of Cr^{2+} as an external reducing agent.[16] Peters, Artero, and Reisner independently investigated the electrocatalytic H_2 evolution by cobaloxime derivatives in an acidic organic medium.[17–19] Their success revived the research on oxygen-tolerant cobaloxime-based HER activity on both photocatalytic and electrocatalytic fronts. However, the limited catalytic efficiency, long-term aqueous instability, and loss of catalytic activity under acidic aqueous conditions have raised serious questions on the potential of these cobaloximes for large-scale applications. A similar roadblock was also observed for Ni-bis-(diphosphine)-based Dubois catalysts, which was resolved by the rational incorporation of extended features of enzyme architecture into their periphery of the Ni-core.[20,21] Buoyed by this success of such unconventional enzyme-inspired catalyst design, researchers have also amended outer coordination sphere features around the cobaloxime core. This innovative track of catalyst design technique was the key to the formation of a new genre of cobaloxime catalysts that resuscitates the cobaloxime as a viable option for renewable energy research. The simple, robust, and synthetically maneuverable structure of the cobaloxime core has allowed researchers to optimize the combinations of ingredients for photocatalytic HER, analyze the catalytic pathways during the electrocatalytic H_2 evolution, and explore the effect of extended enzyme-inspired features, which are discussed in detail in the following sections.

Photocatalytic HER activity by cobaloximes

The photocatalytic HER activity is typically driven by collaboration between three independent ingredients: (i) the photosensitizer (PS), (ii) the catalyst, and (iii) the sacrificial electron donor (ED). Here, our discussion will be limited to those systems where a cobaloxime derivative plays the catalytic role. Depending on the nature of the photosensitizer (PS), we have further fragmented our discussion into sections: (i) inorganic noble-metal-based PS, (ii) inorganic non-noble-metal based PS, (iii) organic PS, and (iv) nanomaterial-based PS. The robust nature, synthetic flexibility, and chemical property tunability of the cobaloxime core made it a popular choice for screening the photocatalytic efficiency of an array of photosensitizers under a wide chemical space.

Noble metal-based photosensitizer

As mentioned earlier, photocatalytic hydrogen production can be obtained by using these cobaloximes in the presence of a photosensitizer (PS) and a sacrificial electron donor.[22] The majority of such early studies reported the utilization of expensive Ru/Pt/Ir-based photosensitizers for light-harvesting (Fig. 2 and Table 1).[23–26] Due to the limited water solubility of typical cobaloximes, organic solvents remained the primary choice of medium for photocatalytic HER investigation. The photocatalytic activity is conventionally reported with the parameter turnover number (TON), where the amount of H_2 produced during the experiment is measured against the concentration of PS or cobaloxime catalyst $\left[\mathrm{TON} = \frac{\text{Amount of } H_2 \text{ produced}}{\text{Amount of PS or catalyst present}}\right]$. In one of the first examples, considerable photocatalytic H_2 production was observed for the [$Co(DH)_2$] complex in the presence of $[Ru(bpy)_3]^{2+}$-PS **(7)** following 1 hour of irradiation (TON ~ 38 *vs.* PS). The aero-sensitivity and catalytic performance were improved with specific functionalization of the bipyridyl moiety at the 4,4′-position by methyl, nitrile[27] or carbene[28] groups.[25] Platinum (Pt)-based PS and Pt-acetylide **(8)** allowed for the prolonged irradiation and presence of external water during an analogous experimental setup, which significantly improved the TON.[29] The improvement in TON was continued with the use of an extended π-conjugated Pt-based PS **(9)**.[24] One of the highest initial-stage photocatalytic HER rates has been observed for $[Ru(bpy)_3]^{2+}$ among the cobaloxime-noble-metal PS dyad, although its long-term stability is poor in contrast to [$ReBr(CO)_3(bpy)$] **(10)**. Probst *et al.* reported one of the first rhenium-based complexes for photocatalytic HER using triethanolamine (TEOA) as a sacrificial electron donor.

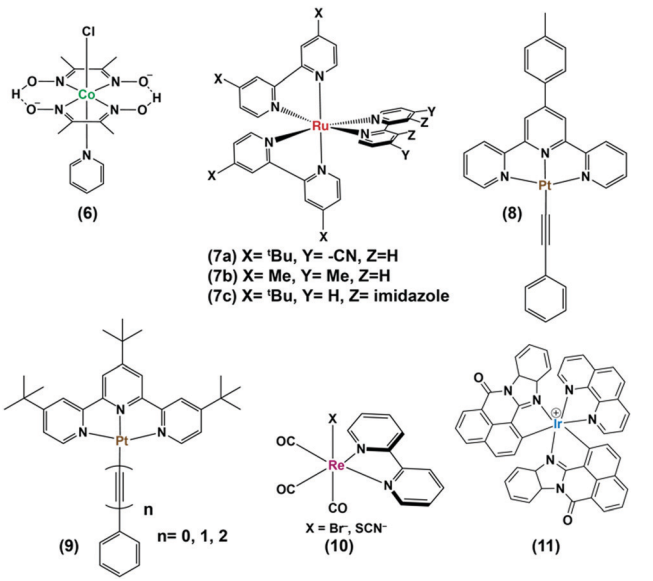

Fig. 2 Structures of various noble metal-based photosensitizers **(7–11)** used with cobaloxime derivatives, such as **(6)** for photocatalytic hydrogen evolution in homogeneous condition.

 This journal is © The Royal Society of Chemistry 2020

Published on 05 June 2020. Downloaded on 1/24/2026 11:49:52 AM.

Table 1 Comparison of photocatalytic HER performance using noble metal-based photosensitizers in cobaloxime solution

Cbx[a]	PS[b]	Solvent/proton source	ED[c]	λ_{ex} cut off (nm)	Irr. time (h)	TON (*vs.* PS)	Ref.
(6)	**(7)**	2 : 1 CH_3CN/H_2O	DMT[d]	452	10	91	23
(2)	**(11)**	2 : 1 CH_3CN/H_2O	DMT	452	10	352	23
(2)	**(7a)**	Methanol	TEA[e]	470	20	470	27
(2)	**(7b)**	9 : 1 CH_3CN/H_2O	AscH[f]	470	24	792	28
(6)	**(7c)**	1 : 1 CH_3CN/H_2O	AscH	400	1	214	25
(6)	**(8)**	3 : 2 CH_3CN/H_2O	TEOA[g]	410	10	400	29
(6)	**(9)**	1 : 1 CH_3CN/H_2O, pH 8.5	TEOA	420	3.5	789	24
(2)	(**(10)**, X = Br)	DMF/AcOH	TEOA	415	9	150	30
(2)	(**(10)**, X = NCS)	DMF/HBF_4	TEOA	476	120	2000	31

[a] Cbx: cobaloxime derivative. [b] PS: photosensitizer. [c] ED: electron donor. [d] DMT: *N*,*N*′-dimethyl-*p*-toluidine. [e] TEA: triethylamine. [f] AscH: ascorbic acid. [g] TEOA: triethanolamine.

After 9 h of irradiation in DMF solution, $[Co(DH)_2]$ displayed 150 TON (250 W, $\lambda > 400$ nm) in the presence of Re-based PS.[30] However, the use of such Re-based PS was futile as it exhibited significant degradation over time.[30] The substitution of the labile Br^- with NCS^- improved the stability of this Re-complex that resulted in better photocatalytic hydrogen production.[31] Castellano and co-workers developed a cyclometalated Ir-based photosensitizer **(11)**, along with cobaloxime, for photocatalytic H_2 production in near neutral condition.[23]

Continuing the search for a stable photocatalytic system, the axial pyridine ligand was used as a linker to covalently connect noble metal-based photosensitizers.[32–35] Fihri *et al.* prepared a supramolecular assembly, where a ruthenium-tris-di-imine PS was coupled to a cobaloxime core (**(12–13)**, Fig. 3) through the axial pyridine. This modification positively shifted the $Co^{II/I}$ reduction potential by ~80 mV, but it eventually slowed down in the longer run.[36] After 15 hours of irradiation ($\lambda > 350$ nm), a TON of 103 (measured *vs.* cobaloxime catalyst) was observed in the presence of 100 equivalents of Et_3N (electron donor) and Et_3NHBF_4 (proton source).[33]

Sun and co-workers improvised this strategy to incorporate an amide linker at a variable length between the axial-pyridine and PS (**(14)**, Fig. 3). The presence of a methylene spacer between the linker and pyridine turned out to be a critical stabilizing factor, as it amplified the TON by ~1.5 times compared to the control complex during a 4 h irradiation (Xe lamp, 500 W, $\lambda > 400$ nm) in acetone. It is believed that this unconjugated methylene spacer possibly impedes the back electron transfer from the reduced metal to the PS to improve the overall photocatalytic efficiency.[34]

The Ir-polypyridyl photosensitizer-based supramolecular PS–cobaloxime dyad **(15)** yielded a comparatively higher TON (~140; after 8 h of irradiation in an acetone solvent with a Hg lamp (150 W, $\lambda > 380$ nm)).[32] Analogous heteroleptic Ru(II)-photosensitizer-bound cobaloxime assemblies (**(16–19)**, Fig. 3) were also developed to harvest the longer wavelengths due to their broad red-shifted emission.[37] However, they exhibited poor photocatalytic HER (4 h irradiation, TON: 9) that was attributed to the low quantum yield and short-lived excited states of those heteroleptic PS-catalyst dyads.[38] Further studies with such Ir-containing multi-component PS–cobaloxime assemblies (**(20)**, Fig. 4) revealed low efficiency, albeit a higher catalytic turnover with prolonged irradiation.[39,40] In a different approach, Mulfort and co-workers targeted the equatorial sites of the cobaloximes to append the light-harvesting Ru-PS component (**(21–22)**, Fig. 4). Through this transformation, they were even able to identify the key photosynthetic charge-separated intermediate (Co^I) for ~26 ps.[41]

Most of the above-mentioned photocatalytic H_2 production reactions, containing a noble-metal-based PS and cobaloxime catalyst, suffered a setback when water was added to the reaction medium. Eisenberg and his team utilized a mixture of Pt-based PS $[Pt(ttpy)(C{\equiv}CPh)]ClO_4$ (ttpy = 4′-*p*-tolyterpyridine) and cobaloxime derivative $[ClCo(DH)_2(methylisonicotinate)]$ to demonstrate effective H_2 production even in a 3 : 2 acetonitrile : water mixture (200 W mercury xenon lamp, $\lambda > 410$ nm).[42]

It can be summarized here that Ru- and Ir-based photosensitizers exhibited better photocatalytic HER in partnership

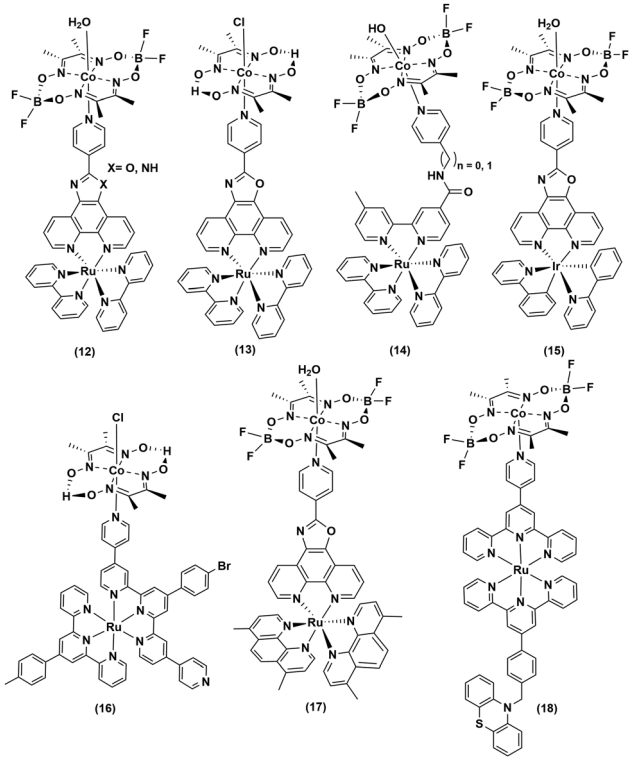

Fig. 3 Noble metal-based photosensitizer–cobaloxime dyads for photocatalytic hydrogen evolution.

Published on 05 June 2020. Downloaded on 1/24/2026 11:49:52 AM.

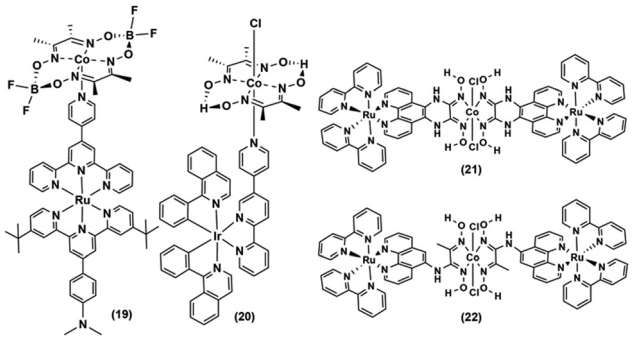

Fig. 4 Various noble metal-based PS-axial- **(19–20)** and -equatorial-linked **(21–22)** cobaloximes.

Table 2 Comparison of the photocatalytic HER for covalently linked noble metal photosensitizer and cobaloxime dyads

Cbx–PS[a]	ED[b]	λ_{ex} cut off (nm)	Irr. time	TON *vs.* PS	Ref.
(12)	TEA[c]	350	4 h	56	33
(13)	TEA[c]	350	4 h	17	33
(**(14)**, n = 0)	TEA[d]	400	8 h	38	34
(**(14)**, n = 1)	TEA[d]	400	8 h	48	34
(16)	TEOA[c]	450	15 days	764	38
(15)	TEA[d]	380	15 h	210	32
(17)	TEA[d]	380	15 h	103	32
(19)	TEOA[c]	525	2.5 h	14	37
(20)	TEOA[e]	595	18 h	180	39

[a] Cbx–PS: cobaloxime–photosensitizer conjugate. [b] ED: electron donor; solvents. [c] DMF. [d] Acetone. [e] Acetonitrile.

with the cobaloxime catalyst, and the reactivity improved significantly when both PS and catalyst modules were connected *via* covalent linker (Table 2).

Non-noble metal-based photosensitizers

The low abundance and high expense of noble metals compelled the researchers to explore the possibility of employing non-noble metal-based photosensitizers for photocatalytic H_2 production with cobaloximes (Fig. 5 and 6). The presence of Mg-based chlorophylls and their active participation in the photo-harvesting process inspired the synthesis of magnesium (Mg)-based synthetic porphyrins. Following the similar synthetic

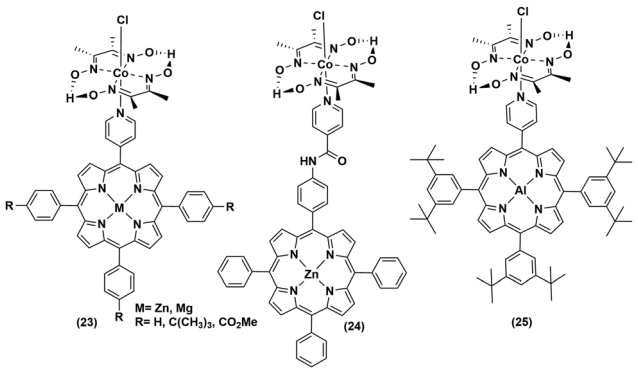

Fig. 5 Non-noble metalloporphyrin-linked cobaloximes for photocatalytic hydrogen evolution.

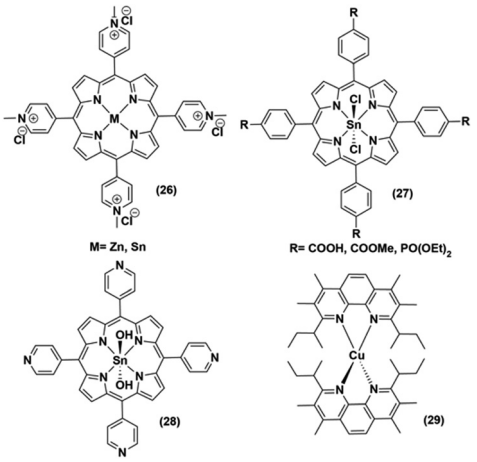

Fig. 6 Non-noble metal-based PS used with various cobaloximes for photocatalytic hydrogen evolution.

methodology, zinc (Zn)-based porphyrin analogues were also prepared. Zinc porphyrins illustrated higher photocatalytic efficiency compared to the magnesium counterpart when they were appended with the cobaloxime *via* axial ligation (**(23)**, Fig. 5). This higher efficiency is attributed to the possible pre-coordination of trimethylamine (TEA) to the zinc porphyrin that facilitates inner sphere electron transfer (ET) from TEA to PS.[43] In a follow-up study, an amide spacer was included in the linker that quenched the electron transfer rate, causing the irradiation to slow down the overall photocatalytic HER activity by this modified Zn-porphyrin–PS–cobaloxime assembly (**(24)**, Fig. 5).[44]

It is noteworthy that axial imidazole-linked cobaloximes display superior photocatalytic HER activity in comparison to axial pyridine-linked cobaloximes.[45] Natali and co-workers developed *in situ* Al-porphyrin linked to the hydrogen-bridged cobaloximes (**(25)**, Fig. 5) through the pyridyl group, which exhibited limited photocatalytic HER [TON_{max} = 352 (*vs.* PS, 175 W Xe-arc, $\lambda > 400$ nm).[46] In a parallel study, tin-based porphyrins (**(26–28)**, Fig. 6) were also probed for the role of PS under similar conditions. Interestingly, photocatalytic H_2 production was observed only in the presence of the water-insoluble tin-porphyrin derivative [$SnTPyP(OH)_2$] (**(28)**, Fig. 6), but not with the water-soluble tin-porphyrin chloride [SnTmPyP] (**(26)**, Fig. 6).[47] Probst *et al.* reported a water-soluble Sn-porphyrin system (**(27)**, Fig. 6) that was active as a PS for photocatalytic H_2 production. However, its short-lived excited state reduced the overall catalytic efficiency.[48] Later, several other zinc-porphyrin or -corrole chromophores were screened with cobaloximes in aqueous or aqueous–organic solvent mixtures.[49,50] In recent years, the earth-abundant copper-based $[Cu(I)(dsbtmp)_2]^+$ (dsbtmp = 2,9-di(*sec*-butyl)-3,4,7,8-tetramethyl-1,10-phenanthroline) PS (**(29)**, Fig. 6) was also developed. This Cu(I)–PS exhibited only moderate photocatalytic H_2 production in the presence of cobaloxime (TON ~ 35 *vs.* cobalt catalyst, λ_{ex} 450 nm), although the photosensitizer retained activity over five days and six cycles of experiments under visible light.[51] Analogously, tellurium (Te)-linked cobaloximes were also generated, but it showed negligible hydrogen evolution even in the presence of multiple light-harvesting components.[52]

This journal is © The Royal Society of Chemistry 2020

Published on 05 June 2020. Downloaded on 1/24/2026 11:49:52 AM.

Table 3 Comparison of non-noble metal-based photosensitizer–cobaloxime assemblies

Catalyst	PS	λ_{ex} cut off (nm)	Irr. time (h)	TON *vs.* PS	Ref.
(**23**, M = Zn)[a]		400	5	22	43
(**23**, M = Mg)[a]		400	3	2	43
(24)[a]		400	5	5	44
$[ClCo(DH_2)_2(pyr_{CN})]$	(**26**, M = Zn)[b]	440	11	77	22
$[ClCo(DH_2)_2(pyr_{CooH})]$	$[Zn(TmPyP)]^b$	440	26	40	22
$[ClCo(DH_2)_2(pyr)]$	$[Zn(TmPyP)]^b$	440	63	320	22
$[ClCo(DH_2)_2(pyr_{SH})]$	$[Zn(TmPyP)]^b$	440	43	425	22
$[ClCo(DH_2)_2(pyr_{Me})]$	$[Zn(TmPyP)]^b$	440	40	443	22
$[ClCo(DH_2)_2(Im)]$	$[Zn(TmPyP)]^b$	440	50	565	22
$[ClCo(DH_2)_2(Im_{Me})]$	$[Zn(TmPyP)]^b$	440	50	1135	22
(2)	$[Zn(TmPyP)]^b$	440	23	290	22
(6)	**(28)**[b]	440	140	150	47
$[ClCo(DH_2)_2(pyr_{COOH})]$	$[Sn(TPyP(OH)_2)]^b$	440	100	40	47
$[ClCo(DH_2)_2(Im_{Me})]$	(27, R = COOMe)[b]	440	48	128	58
$[ClCo(DH_2)_2(Im_{Me})]$	[27, R = $PO(OEt)_2$][b]	440	48	48	58
(25)[c]		400	2	280	46
(6)	**(29)**[d]	452	20	70	51
(6)	((**27**), R = COOH)[e]	390	20	20	48

Solvent/electron donor. [a] THF–H_2O (8 : 2)/TEA. [b] 1 : 1 CH_3CN–H_2O/TEOA. [c] 7 : 3 acetone–H_2O/ascorbic acid. [d] 1 : 1 CH_3CN–H_2O/DMT. [e] pH 8.5/TEOA.

Hence, it can be mentioned here that despite the evolution of a variety of non-noble metal-based photosensitizers, they were unable to match the excellent photo-driven cobaloxime-catalysed HER activity showcased by noble metal (especially Ru and Ir)-based PS assemblies (Table 3). However, the photo-bleaching of these inorganic photosensitizers under pro-longed irradiation has cast serious doubts on their long-term applications.

Organic photosensitizer

The plausible role of organic dyes as a photosensitizer was also probed in detail in the pursuit of an artificial photosynthetic assembly. Various organic dye molecules containing diverse categories of functionalities, such as boron dipyrromethane (BODIPY),[53] Rose Bengal,[54] Rhodamine,[55] Acriflavin,[56] and Eosin,[57] represent the face of organic dye instigated photocatalytic HER research using cobaloxime derivatives as a diagnostic tool (Fig. 7). Analogous to their metal-based PS counterpart, the organic dye molecules were also utilized in two distinct formats for cobaloxime-derived photocatalytic HER: (i) untethered free organic dye PS and cobaloxime in solution, and (ii) covalently linked organic dye–cobaloxime dyads. We have reviewed the consistent growth in either of those approaches in the following sections.

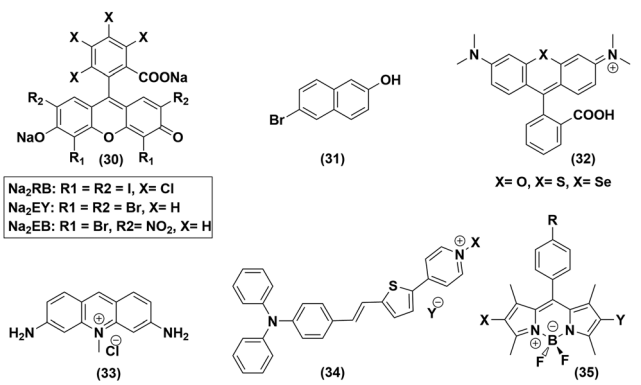

Fig. 7 Various organic dye molecules used in the homogenous solution phase, along with cobaloximes, for photocatalytic hydrogen evolution.

Untethered free organic dye as photosensitizer

Xanthene-based dyes are one of the widely explored photoactive molecules, and were chosen for the initial photocatalytic studies to play the role of a PS. When the basic xanthene skeleton was mixed along with cobaloxime in solution, it failed to produce any H_2 under illumination. A close look into this failed experiment revealed that the excited state of the PS should be a long-lived one to support such a bimolecular photocatalytic reaction. The photophysical properties of xanthene molecules suggest that the lifetime of the photo-excited state can be prolonged by facilitating the intersystem crossing (ISC) process with the introduction of heavy atoms like halogens. With the use of Eosin and Rose Bengal (RB) as PS ((**30**), Fig. 7), the successful photocatalytic H_2 evolution validated that hypothesis.[59] Complex **6** exhibited TON = 900 (*vs.* catalyst, pH 7, 5% TEOA, 1 : 1 CH_3CN/H_2O, $\lambda > 410$ nm, 12 h irradiation, excess ligand) in the presence of Eosin-Y (EY^{2-}). However, this photocatalytic activity was hampered whether in acidic or basic medium.[57] The BF_2-bridged cobaloximes $[Co^{II}(DBF_2)_2]$ exhibited better stability compared to the hydrogen-bonded cobaloximes when these xanthene derivatives were used as PS. The annulated cobaloxime $[Co^{II}(DBF_2)_2]$ displayed a TON of 32 with maximum activity in basic medium (pH 10) in the presence of Rose Bengal PS (500 W Xe lamp, 5 h irradiation, 10% TEOA, $\lambda > 400$ nm).[54] The photo-activated proton movement in 6-bromo-2-napthol **(31)** was also employed for cobaloxime-generated photocatalytic H_2 production, which highlights the versatility of the cobaloxime core in screening different PS sources.[60] The photocatalytic HER activity was boosted when the O atom in the heterocycle of xanthine framework was replaced with heavier chalcogens S and Se

Table 4 Untethered organic dye PS and cobaloxime assemblies for photocatalytic HER activity

Catalyst	PS	λ_{ex} cut off (nm)	Irr. time (h)	TON *vs.* PS	Ref.
(6)	RB^{2-} [a]	400	5	321	54
(6)	(**(32)**, X = Se)[b]	520	5	3737	55
(6)	**(33)**[c]	420	2	110	56
(6)	EY^{2-} [b]	450	30	220	57
(6)	RB^{2-} [b]	450	5	540	59
(3)	**(31)**[b]	226	0.75	—	60
(6)	(**(35)**, X = Y = I, R = COOH)[d]	420	9	132	64
Bis-pyridyl-propane-$[Co(DH_2)_2]_2$	EY^{2-} [b]	420	2	562.5	62
4-4′-bpy-$[Co(DH_2)_2]_2$	EY^{2-} [b]	420	10	160	63 and 69
$[Cl\text{-}Co(DH_2)_2(pyrm\text{-}EtCOOH)]$	EY^{2-} [b]	400	5	444	67

Solvent/electron donor. [a] 2 : 1 CH_3CN–H_2O/TEA. [b] 1 : 1 CH_3CN–H_2O/TEOA. [c] 3 : 1 DMF–H_2O/TEOA. [d] 3 : 2 CH_3CN–H_2O/TEOA.

Published on 05 June 2020. Downloaded on 1/24/2026 11:49:52 AM.

(**(32)**, Fig. 7). The S- and Se-substituted Rhodamine (RB) exhibited excellent cobaloxime-catalysed photo-driven H_2 production with TON values of 1700 and 5500, respectively (5% TEOA, 1 : 1 CH_3CN/H_2O, pH 7, 520 nm LED, 0.15 W).[55] The use of acriflavine **(33)** and pyridinium-based donor–π–acceptor assemblies **(34)** as the photosensitizer, along with cobaloxime, also exhibited photocatalytic H_2 production.[56,61]

The variable combinations of cobaloxime and xanthine-based dyes allowed the researchers to have a glimpse of the importance of the sacrificial electron donor on the photocatalytic HER (Table 4). It was found that, in the presence of triethanolamine (TEOA), the efficiency of photo-generated H_2 production follows the trend: EY^{2-} (alcohol) > EY^{2-} (water) > HF (halogenated fluorescein) > EB^{2-} (Eosin-Blue) > RB^{2-},[62] while it was altered when triethylamine (TEA) donated an electron: EY^{2-} > RB^{2-} > EB^{2-}.[63] Hence, Eosin-Y (EY^{2-}) and TEOA turned out to be one of the best PS-sacrificial electron donor recipes for cobaloxime-derived photocatalytic HER, where a TON of 562 (5% TEOA, λ > 420 nm, 1 : 1 CH_3CN/H_2O) was observed. The halogenated aza-/*meso*-BODIPY dyes (**(35)**, Fig. 7) represent another section of organic dyes that were extensively examined with cobaloximes. BODIPY PS typically operates in neutral or near basic-neutral media with a maximum photocatalytic efficiency at pH 8.5.[64,65] Recently, Sun and co-workers incorporated an 8-hydroxylquinoline group in the *meso*-position of iodinated BODIPY, which was able to reduce the proton, even under acidic medium, in the presence of complex **(6)** and ascorbic acid as the catalyst and electron donor, respectively.[66]

In a similar manner, the cobaloxime motif was also varied to enhance the photo-driven H_2 production in the presence of an identical PS (EY^{2-}). Initially, carboxylic acid groups (–COOH) were appended at the variable position of the axial pyridine ligand of the complex **(6)** molecule. The detailed studies displayed a better catalytic response from a *meta*-carboxylic acid bound complex compared to the *para*-substituted analog. On the other hand, the inclusion of ester functionality reduced the photocatalytic HER to emphasize the possible role of these peripheral functionalities in proton movement and electron distribution during photocatalysis.[67] Recently, our group also observed analogous results when such protic group substitution was performed on the axial imidazole (Im) ligand of the $[ClCo(DH_2)_2(Im)]$ molecule. The presence of multiple interactive basic functionalities and their fluxional dynamics around the cobalt core transpired to be an essential modulating factor for the photocatalytic activity of cobaloximes.[68] Additionally, the use of a self-assembled multinuclear cobaloxime[62] or inclusion of a 4,4′-bipyridine ligand to the cobaloxime core exhibited improved photocatalytic efficiency in comparison to the unsubstituted mononuclear cobaloxime motif.[69]

However, none of these untethered combinations of organic dye and cobaloxime derivatives were primed for inclusion in large-scale usage photo-harvesting procedures due to their long-term instability, especially in water-blended media.

Covalently linked organic dye–cobaloxime dyad

In an attempt to improve the long-term stability and raise the photocatalytic efficiency, the organic dyes were covalently anchored with cobaloxime to generate a series of organic PS-catalyst assemblies (Fig. 8 and Table 5). First, BODIPY dyes were tethered to the axial position of $[Co(DH_2)_2]$ through the *meso*-positioned pyridyl group (**(36–38)**, Fig. 8). Even with the variation of the electron-donating and -withdrawing substituents on the BODIPY motif, these adducts demonstrated poor reactivity.[70] However, the inclusion of heavy atoms like halides was able to enhance the photocatalytic H_2 production to reach a TON of 85 (5 h Irr, 4 : 1 CH_3CN/H_2O, pH 8.5).[71] The efficiency of such light-activated HER improved further with the inclusion of thienyl functionality to the BODIPY–cobaloxime dyad.[72] Despite this initial success, the instability of these adducts in aqueous blended solvents continued to impede their durability.[73] The reactive Co–N(pyridyl) bond is believed to be the primary reason for the instability of the BODIPY–cobaloxime adducts, especially under irradiation.[74]

The activity was improved slightly when the triphenylamine-vinylthiophene-pyridine chain (**(39)**, Fig. 8) was used as a donor–π-linker–acceptor triad.[61] Following the footsteps of BODIPY, Eisenberg *et al.* linked amido-fluorescein to the axial position of cobaloxime (**(40)**, Fig. 8). This amido-fluorescein–cobaloxime adduct exhibited approximately three-fold improvement in photocatalytic HER activity compared to the untethered components under analogous reaction conditions.[75] The Wasielewski group developed a rational model of a donor–linker–acceptor-$[Co(DBF_2)_2]$ cobaloxime assembly framework, without the presence of any heavy atom, to improve the transfer of the photoactivated electron. In this strategy, they synthesized

 This journal is © The Royal Society of Chemistry 2020

Published on 05 June 2020. Downloaded on 1/24/2026 11:49:52 AM.

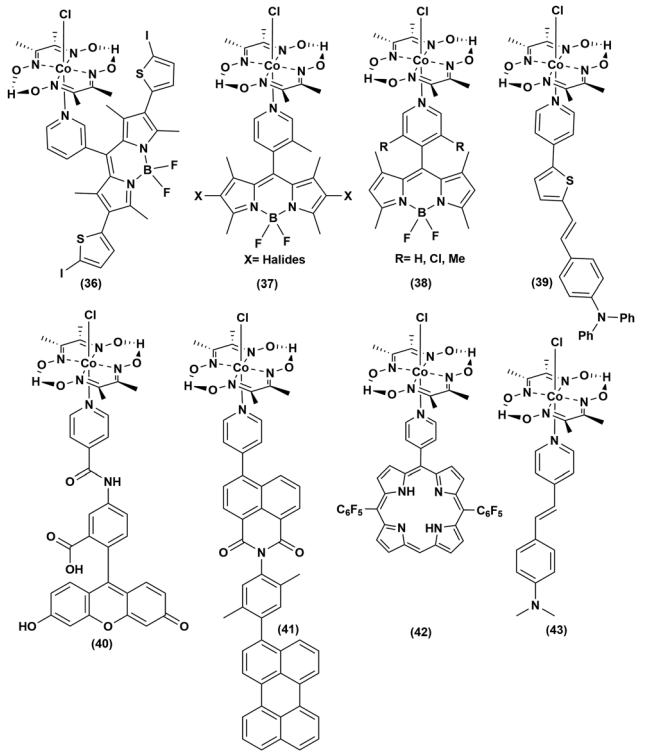

Fig. 8 Metal-free organic dye-linked photosensitizer–cobaloxime conjugates for photocatalytic hydrogen evolution.

a molecule containing perylene, xylene and pyridyl-substituted 1,8-naphthalimide as a donor, bridge and acceptor, respectively, along with a $[Co(DBF_2)_2]$cobaloxime core to achieve moderate photocatalytic HER activity (**(41–42)**, Fig. 8).[76] In a recent study, our group simplified the donor–linker–acceptor chain by using a pyridinyl derivative of a stilbene motif (**(43)**, Fig. 8). Although this $[ClCo(DH_2)_2$pyridnyl-stillbene] adduct was able to exhibit photocatalytic H_2 evolution even under natural sunlight, the overall photocatalytic efficiency and long-term aqueous stability remained poor.[77]

Nanomaterial-based photosensitizer

An ideal photocatalytic assembly should exhibit the following properties to fulfill the demands of harsh practical applications: (i) the PS component should be stable under prolonged irradiation in aerobic conditions, (ii) the catalyst module should be able to produce H_2 from the ubiquitous source of protons, *i.e.*, water. Hence, the generation of a robust photocatalytic assembly, operational in pure aqueous media, remains the final frontier for their practical applications. As mentioned in the earlier sections, the rational utilization of the cobaloxime motif allowed the scientists to screen an array of photosensitizers, ranging from inorganic to organic dye molecules, in the pursuit of an optimized photocatalytic H_2 production assembly. Although some of those dye molecules exhibited considerable H_2 evolution in tandem with cobaloxime, the overall effectivity of such combinations (in either tethered or untethered forms), especially in the presence of water, were low due to the long-term instability of the dye molecules. In this scenario, the semiconductor materials emerged as a possible solution for this conundrum owing to their robust photophysical properties, where it can play the role of a charge mediator between PS and catalyst, while stabilizing the dye molecules under photocatalytic conditions.

Reisner *et al.* employed the resilient TiO_2 nanoparticle (TiO_2 nP) as a mediator for immobilizing both cobaloxime $[ClCo(DH)_2$(pyridyl-4-hydrophosphonate)] (CoP) and $[Ru(bpy)_2$-(bpy-phosphonate)$^{2+}$] (RuP) PS *via* phosphonate–TiO_2 binding. The CoP–TiO_2 nP–RuP combination exhibited significant photocatalytic H_2 production [400 mmol H_2 h^{-1} (g TiO_2)$^{-1}$] in neutral aqueous conditions (pH 7, in the presence of TEOA) (Fig. 9A). Here, the conduction band of the TiO_2 nP was believed to facilitate the fast movement of charge carriers from RuP to the CoP motif. Despite expanding the reactivity in pure aqueous solution, the photocatalytic H_2 evolution by this assembly slows down after 2 hours, and completely ceases after 8 hours under continuous irradiation.[78]

Licheng Sun and team designed an organic dye-sensitized photoelectrochemical (PEC) cell that can perform water splitting under neutral aqueous (pH 7) conditions using visible light. This PEC cell consisted of two parts: (i) photoanode (for water splitting), and (ii) photocathode (for hydrogen generation). A cobalt catalyst Co1 $[Co(DBF_2)_2(H_2O)_2]$ was directly connected to the semiconductor-based photocathode (p-type NiO) surface with phosphoric acid linker along with an organic dye P1, which acted as a photosensitizer (Fig. 9B). This photocathode produced a decent amount of hydrogen upon irradiation.[79] However, scaling up such NiO film is an issue, which prevented a higher amount of catalyst and dye loading for improved H_2 production. The poor charge carrier property of the NiO surface also negates their

Table 5 Directly linked organic dye PS–cobaloxime assemblies for photocatalytic HER activity

Catalyst–PS conjugates	Solvent	ED[a]	λ_{ex} cut off (nm)	Irr. time	TON *vs.* PS	Ref.
Bis-thienyl-BODIPY-$Co(DH_2)_2$	8 : 2 CH_3CN–H_2O	TEA	420	8 h	5.6	53
(**(37)**, X = I)	3 : 2 CH_3CN–H_2O	TEOA	525	17 h	30.9	71
(36)	4 : 1 CH_3CN–H_2O, pH 8.5	TEOA	420	10 h	73	72
3-pyr-*meso*-$BODIPY_{Iodine}$-$Co(DH_2)_2$	24 : 1 CH_3CN–H_2O	TEOA	420	5 h	85	73
(39)	3 : 1 CH_3CN–MeOH	TEOA	455	9 days	122	61
(40)	24 : 1 CH_3CN–H_2O	TEOA	520	28 h	32	75
(41)	DCM[b]	TEA	400	2 h	—	76

[a] ED: electron donor. [b] DCM: dichloromethane.

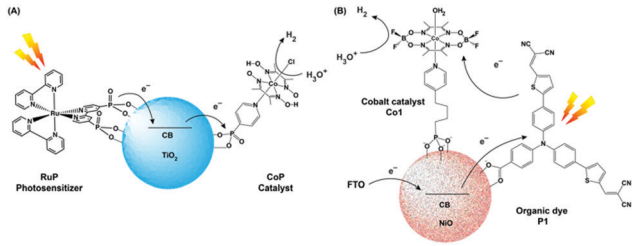

Fig. 9 (A) Schematic representation of photocatalytic H_2 production TiO_2 NPs containing a covalently attached cobalt catalyst (CoP) and a ruthenium photosensitiser (RuP). (B) Representative figure of the photocathode containing organic dye P1 and cobaloxime catalyst Co1 on the NiO surface. The figures are redrawn from ref. 78 and 79 respectively.

long-term usage.[80] Recently, Artero and co-workers have improved the charge transfer between the semiconductor and catalyst by introducing a Ru-diacetylide-spacer between them.[81] In a parallel set of studies, photoactive nanomaterials were used that can directly instigate light-driven HER with the cobaloxime catalyst. For this purpose, a range of materials were used, including graphite-like C_3N_4 (cobaloxime bound *via* π–π stacking through a pyrene tail),[82] CdS quantum dot (containing cobaloxime film on its surface),[83] and the azine-linked N_2-based covalent organic framework (COF) (cobaloxime present in the cavity).[84] All of these materials exhibited moderate photocatalytic HER activity mostly in the organic/water mixture.

Turner and co-workers further modified the photoelectrode design, and used the atomic layer deposited (ALD) TiO_2-modified p-$GaInP_2$ for this purpose. In a sequential synthetic step, cobaloxime [$ClCo(DH)_2$(pyr-COO^-)] was immobilized on the TiO_2 terminal of the photoelectrode surface *via* carboxylate functionality. This modified electrode illustrated excellent photo-electrocatalytic H_2 production activity (TON 139 000 and average TOF of 1.9 s^{-1}) during a 20 h period of 1 sun illumination in basic aqueous media (pH 13). As mentioned earlier, this system required the push of electrons from the electrode surface (which was held at 0 V *vs.* RHE), and its reactivity was limited to strong alkaline conditions. The photocurrent density for this assembly decreased rapidly (~50%) over the first 4 hours of the experiment to raise its long-term instability issue.[85] The detachment of the cobalt catalyst from the TiO_2 surface is believed to be the possible reason for this instability.[86]

In this section, we have established that the presence of a semiconductor surface can play two crucial roles for cobaloxime-based photocatalytic H_2 production reactions. First, the surface immobilization of PS and catalyst moieties ensure that they remain in close distance, which is essential for the rapid charge transfer process following photo-excitation. Second, the electroactive semiconductor surface can be utilized for modulating the potential of the surface to drive the photocatalytic reactions in the desired direction. The second factor even allowed us to probe the otherwise unexplored photocatalytic water oxidation pathway by a cobaloxime derivative [$ClCo(DH)_2$(pyr-cysteamine)], which was immobilized on the TiO_2–gold nanomaterial surface.[87]

Electrocatalytic HER activity by cobaloximes

As mentioned earlier, cobaloxime can act as a functional model for the hydrogenase enzyme, where the electron-transporting [Fe_4S_4] clusters can be mimicked by an electrode surface (Fig. 1B). The catalytic efficiency of the cobaloxime derivatives can be monitored as a function of the applied potential on the electrode surface (*i.e.*, the energy of the electron) and the resultant catalytic current (that is directly proportional to the catalytic rate).[88–90] Utilizing the unique structure of the cobaloxime core, researchers have probed the effect of electron-donating/-withdrawing substituents present in the primary coordination sphere and the influence of peripheral proton network *via* electrochemistry experiments. Such electrocatalytic studies have been performed on cobaloxime molecules in two different conditions: homogeneous and heterogeneous. In homogeneous conditions, the catalytic molecule and substrate (H^+ in the case of H_2 production) remain in the solution phase, and it interacts with the solid electrode surface in its electrochemical double layer. On the other hand, the catalyst is immobilized on the electrode surface during the heterogeneous study, while only the substrate stays in the solvent phase. In the following sections, the results from either set of experiments have been analyzed. It is worth mentioning that analogous nickel dimethylglyoximato complexes exhibited moderate HER activity in organic solvents, while they degraded into nanoparticles in aqueous solution under a reducing potential.[91]

Homogeneous electrocatalytic HER

Instability of the basic [$Co(DH_2)_2$] framework led to the development of an air- and moisture-stable N-axial pyridine cobaloxime system. [$ClCo(DH)_2$(pyr)] typically displays a reversible ($Co^{II/I}$) and an irreversible ($Co^{III/II}$) redox reduction feature in dry organic media. Irreversible $Co^{III/II}$ is related to the loss of an axial ligand in the Co^{II} state. The addition of an acid ($Et_3NH^+Cl^-$) in the solution transforms the reversible $Co^{II/I}$ signal into an irreversible one, and the reductive current continues to increase with an increasing amount of acid.[17] Complementary bulk electrolysis (*i.e.*, chronocoulometry) and gas chromatography experiments identified the enhanced reductive response as catalytic hydrogen generation. Complex **(6)** exhibited 85–100% faradaic efficiency (FE) during this electrocatalytic HER during the 2.5 h of bulk electrolysis in dichloromethane (graphite electrode, −0.9 V *vs.* Ag/AgCl).[92]

The initial modifications to the cobaloxime core were executed on the equatorial motif. The substitution of the methyl groups of the dimethylglyoxime moiety with phenyl groups not only reduced the catalytic HER response, but also increased the overpotential requirement (the difference between the applied potential and standard reduction potential for H_2 evolution at the experimental conditions; $\eta = \left|E_{applied} - E^0_{H^+/0.5H_2}\right|$).[93] Interestingly, the overpotential requirement value was lowered when the hydrogen-bonded oxime network was replaced by the BF_2 groups in [$(CH_3CN)_2Co^{II}(DBF_2)_2$] (−0.28 V *vs.* SCE in CH_3CN).[18]

Published on 05 June 2020. Downloaded on 1/24/2026 11:49:52 AM.

This journal is © The Royal Society of Chemistry 2020

Published on 05 June 2020. Downloaded on 1/24/2026 11:49:52 AM.

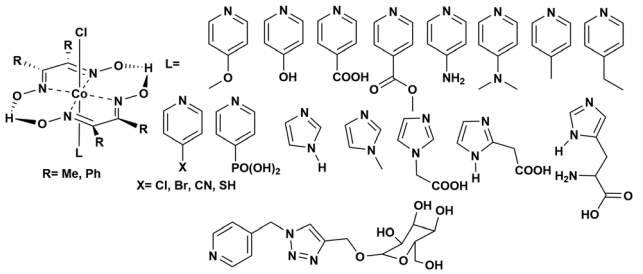

Fig. 10 N-Axial pyridine cobaloxime derivatives used for the study of the electrocatalytic hydrogen evolution reaction.

However, this difluoroboryl annulated complex demonstrated reduced HER activity, and it required the presence of a stronger acid for electrocatalytic H_2 production.[94] As the axial halide ligands are labile in nature, especially in the reduced oxidation states of cobalt, the axial pyridine gained more attention for axial ligand modification. A series of diverse functionalities (such as amine, alcohol, ester, carboxylic acid, thiol, phosphate, alkyl, halide) have been introduced in the axial pyridyl motif to generate a library of axial-pyridine modified cobaloximes (Fig. 10). Reisner and co-workers have developed an electrochemical method, known as "*Electrochemical Molecular Catalyst Screening*" or EMOCS, for studying the electrocatalytic behaviour of such *in situ* generated pyridyl cobaloximes prior to their actual synthesis. This EMOCS method turns out to be a user-friendly screening method for comparing the axial ligand effect on the HER activity of cobaloxime core in analogous conditions.[95] The detailed electrochemical results from these studies revealed a unique structure–function relationship for the axial-pyridine modified cobaloximes. The electron-donating substituents improved the electrocatalytic rate for the cobaloximes, but at the expense of the catalytic efficiency (overpotential also increases). In contrast, the electrocatalytic H_2 production rate was reduced in the presence of an electron-withdrawing group in the axial pyridine, while making it an efficient catalyst (overpotential also decreases). Inclusion of the phosphate derivative in the axial ligand further improves the oxygen-tolerance of the cobaloxime core. However, it exhibited an acute CO poisoning effect.[96,97] The bimolecular cobaloximes, containing an equatorial octamethylene unit, were also prepared *via* the equatorial BF_2 groups as the bridging ligand. However, no significant enhancement in the electrocatalytic performance was noticed in comparison to the mononuclear cobaloxime.[88]

All of the cobaloxime derivatives discussed so far in this section were screened in an organic solvent due to their poor aqueous solubility. Zhang *et al.* introduced a glucose-functionalized pyridine motif to the cobaloximes to improve the water solubility. This modification produced water-soluble cobaloximes that operated under a neutral aqueous medium. However, they lost their catalytic properties as the acidity of the solution increased (pH $\leq$ 5).[98] This loss of activity under acidic conditions is attributed to the cleavage of the oxime-derived hydrogen-bonding network, which acts as the primary protonation site during the electrocatalytic cycle. Hence, the activity of cobaloximes, even in acidic conditions, can be revived with the inclusion of an alternative protonation site. The introduction of an enzyme-inspired outer coordination sphere around the cobaloxime core allowed the presence of such a secondary protonation site that will be discussed in detail in a following section.[99]

Heterogeneous electrocatalytic HER

The cobaloxime motif was immobilized on variable electroactive surfaces in an attempt to improve its electrocatalytic performance compared to the homogeneous conditions. Reisner and co-workers led the research in this front and developed a cobaloxime-*meso*-ITO film (*via* phosphonate group) on an ITO electrode, which exhibited H_2 production at a moderate overpotential. However, the cobaloxime bound on this mesoporous electrode degraded over time.[100] They improved the stability of the surface-bound cobaloxime by using multiwall carbon nanotube (mw-CNT) material. Multiple cobaloxime molecules containing pyrene tails were anchored on the mw-CNT surface through π–π interactions.[101] Artero *et al.* further improvised this approach and prepared a nanohybrid of mw-CNT and cobaloxime using a self-assembled polymeric amphiphile. This amphiphile contained diacetylene (DA) as a hydrophobic tail and a pyridine (pyr) moiety as the polar head, which was directly coordinated to the cobaloxime core (Fig. 11A). A glassy carbon electrode surface was modified with this cobaloxime–CNT hybrid that exhibited 110–120 turnovers for electrocatalytic HER in a neutral aqueous medium. However, this surface-modified catalyst suffered from degradation after 30 min under electrolytic conditions as the unstable cobaloxime leached out from the CNT surface.[102]

Moore and co-workers studied the photoelectrocatalytic behaviour of a cobaloxime catalyst grafted on a p-type gallium phosphide (100) semiconductor *via* polyvinylpyridine (PVP) ligands. This assembly was active for photocatalytic HER activity, which was sensed *via* electrochemistry.[104] They developed the next generation of such modified electrodes by immobilizing cobaloximes on the nanostructured indium tin oxide (nano-ITO) surface *via* in-built polyvinylpyridine (PVP) ligands (Fig. 11B). This nano-ITO was employed as a working

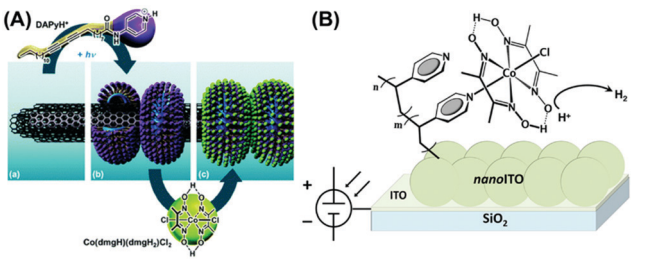

Fig. 11 (A) The self-assembled structure of polymeric amphiphile (DApyr)–cobaloxime–CNT nanohybrid, exhibiting (a) the layers of multi-walled carbon nanotube (CNT), (b) nano-rings generated by the polymeric amphiphile, and (c) the cobaloxime-functionalized nano-hybrid. Reproduced from ref. 102 with permission from The Royal Society of Chemistry.[102] (B) The cobaloxime–PVP polymer-immobilized nano-ITO Electrode surface. Reproduced from ref. 103 with permission from © American Chemical Society, 2016.[103]

Published on 05 June 2020. Downloaded on 1/24/2026 11:49:52 AM.

electrode for the hydrogen evolution reaction in phosphate buffer (pH 7). This heterogeneous assembly displayed a hydrogen production rate of 3 μL min^{-1} cm^{-2} with a relatively lower faradaic efficiency of 50 ± 3%. The calculated TOF for this electrocatalytic HER was 1200 ± 200 h^{-1} per cobalt centre, which is orders of magnitude lower in contrast to analogous cobaloximes in homogeneous conditions.[103] Recently, the Artero group was also able to achieve electrocatalytic HER activity by using a modified electrode containing $CuFe_xO_y$ semiconductor–TiO_2–cobaloxime layers.[105]

Ott and co-workers immobilized a cobaloxime derivative on a metal–organic framework (MOF), and studied its electrochemical behaviour in acetate buffer (pH 4). This catalyst consisted of a 3D MFO UU-100 Co and cobaloxime catalyst with carboxylates as the anchoring groups (Fig. 12). This cobaloxime-grafted MOF generated hydrogen with a faradaic efficiency of 79%, with an average TOF of 1171 h^{-1}. The overall TON of 20 875 was obtained for this catalyst after 18 h of electrocatalysis.[106] The MOF backbone ensured that the cobaloxime motif could be active in a 3D structure, while the robust nature of MOF provided the acid-stability. The porous structure of the catalyst-modified MOF also allowed access to the internally buried catalytic side, while instigating a facile diffusion of the electrolyte and substrates during electrocatalysis. However, the poor charge transfer properties and non-conducting nature of MOF have raised questions on its long-term implementation.[107,108]

Thus, the homogeneous electrocatalytic experiments with cobaloxime derivatives provided us with a deep insight into the structural and electronic factors that regulate their electrocatalytic behaviour. However, the overall catalytic performance (both catalytic rate and overpotential) was inferior compared to the state of the art Ni-bis-(di-phosphine)-based Dubois catalysts.[109] On the other hand, cobaloximes were immobilized on different solid surfaces, including carbon nanotubes, semiconductor nanomaterials, and metal organic frameworks. Although these heterogeneous materials replicated the electrocatalytic HER activity of cobaloximes in heterogeneous conditions, they were unable to improve its long-term durability and catalytic efficiency under practical conditions.

The limited success with the current approaches towards cobaloxime-promoted photocatalytic and electrocatalytic HER activities for extensive industrial-scale usage necessitated a new direction in this research area. The successful evolution of Dubois catalysts indicates that the unconventional enzyme-inspired catalyst design strategy can be a way forward to invigorate the basic cobaloxime core in the first place. In the next step, the improvised cobaloxime derivatives can be investigated for efficient and robust photocatalytic and electrocatalytic H_2 evolution under the most practical conditions.

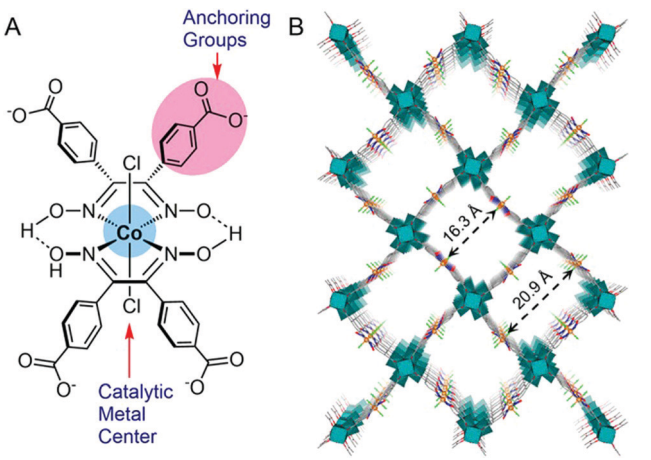

Fig. 12 (A) The basic structure of the cobaloxime derivative containing benzoate substituents that is used as linker in UU-100(Co), and (B) the 3D structural model of the UU-100(Co) MOF with a view along the [001] plane. Reproduced from ref. 106 with permission from © American Chemical Society, 2019. Further permissions related to this figure should be directed to the American Chemical Society.[106]

Enzyme-inspired modifications of cobaloximes

Naturally evolved hydrogenase enzyme has been known to play a critical role in H_2-based metabolism in various life forms for millions of years. All of the different variants of this enzyme contain naturally abundant Fe and Ni in its active site (referred to as [FeFe]- and [NiFe]-hydrogenase). They catalyze H_2 production from water at a rapid rate, while maintaining a low overpotential requirement.[110,111] All of these features have prompted the hydrogenase active site as a popular choice for the development of biomimetic model complexes for artificial hydrogenases.[112] Interestingly, most of the active site models fail to imitate the enzymatic reactivity under practical conditions, which led to the hypothesis that the presence of the protein scaffold around the active site has a significant role in attaining the catalytic excellence.[20] Consequently, several research groups have extended their bio-mimetic design beyond the active site to the secondary and outer coordination sphere features.[20,113] The HER activity by the cobaloxime core is sensitive to its surrounding environment. Hence, it was rationally combined with variable supramolecular scaffolds (proteins/polymers) to probe the effect of secondary and outer coordination sphere features on the cobaloxime-derived HER activity.

A research group led by Utschig and Tiede inserted a cobaloxime motif [$Co(DH)_2$(pyr)Cl, **(6)**] with a natural Photosystem-I (PSI) protein to fabricate a PSI–cobaloxime hybrid (Fig. 13A). This hybrid construct was active for photocatalytic H_2 production in a neutral aqueous solution in the presence of an electron mediator cytochrome *c*6. This particular construct was able to produce 170 mol H_2 per mol of PSI per min that is equivalent to the 50% catalytic rate of an analogous PSI–Pt nanoparticle system, while it outperformed the PSI–hydrogenase hybrid.[114,115] Later, they simplified their construct and removed the bulky PSI protein. In this new assembly, they utilized an electron-transporting ferredoxin (Fd) protein to bridge a synthetic photosensitizer [$Ru(bpy)_3^{2+}$] with the catalytic cobaloxime core [$Co(DBF_2)_2$] (Fig. 13B). This [$Ru(bpy)_3^{2+}$]–Fd–[$Co(DBF_2)_2$]

 This journal is © The Royal Society of Chemistry 2020

Published on 05 June 2020. Downloaded on 1/24/2026 11:49:52 AM.

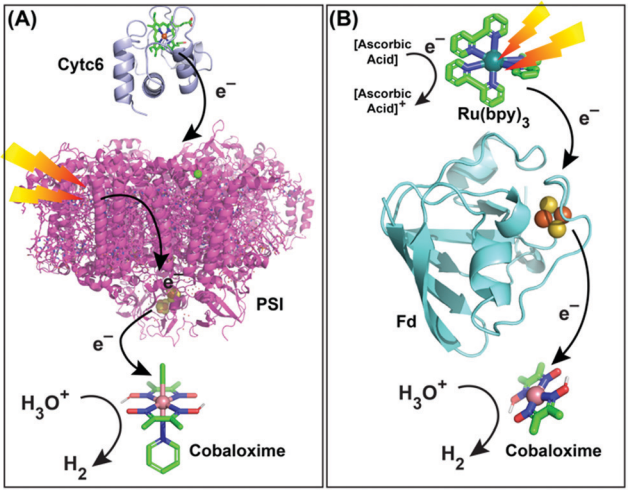

Fig. 13 Photocatalytic HER activity exhibited by (A) the PSI–cobaloxime [Co(dmgH)$_2$(pyridine)Cl] hybrid in the presence of cytochrome *c*6 (Cytc6) as an electron transfer partner, and (B) the [Ru(bpy)$_3^{2+}$]–ferredoxin (Fd)–cobaloxime [Co(dmgBF$_2$)$_2$] assembly in the presence of ascorbic acid as a sacrificial electron donor. These figures are redrawn from ref. 114 and 116. The molecules and proteins are not drawn to scale for clarity.

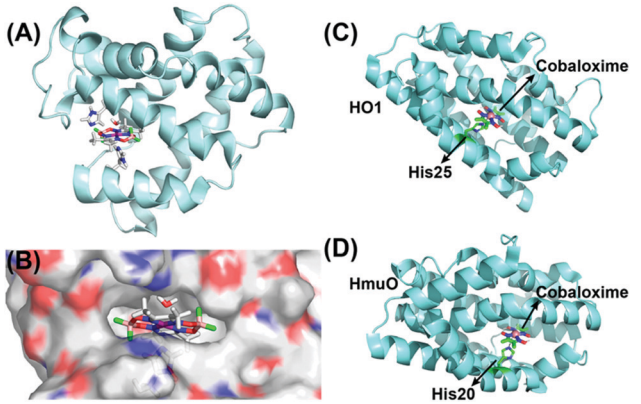

Fig. 14 (A) The QC/MM calculated structure of *Sw*Mb-cobaloxime [Co(dmgBF$_2$)$_2$], and (B) its electrostatic environment around the cobaloxime core. The hydrophilic regions are depicted in red (O atoms) and blue (N atoms), while the hydrophobic regions are displayed in grey. This figure is adapted from ref. 120. Permission was obtained from the © American Chemical Society, 2014. The heme oxygenase-bound cobaloxime structures of (C) HO1–cobaloxime [Co(dmgH$_2$)$_2$], and (D) HmuO–cobaloxime [Co(dmgH$_2$)$_2$]. The black arrows direct the position of the cobaloxime and the protein-derived axial histidine ligands. The cobalt atom is depicted in purple, boron in pink, carbon in green and fluorine in fluorescent green. These figures were redrawn from ref. 121.

hybrid exhibited the production of 60 mol H_2 per mol of [Ru(bpy)$_3^{2+}$] per hour in a neutral aqueous solution upon photoirradiation, which was improved by ~3 times in the presence of the axial pyridine bound cobaloxime.[116,117] In a follow-up study, another [Ru(bpy)$_3^{2+}$]–Fld–[Co(DBF$_2$)$_2$] biohybrid was prepared by replacing the Fd protein with a flavodoxin (Fld) scaffold, which afforded HER activity *via* a different pathway.[117]

As discussed earlier, the inclusion of pyridine or imidazole axial ligands can positively influence the catalytic H_2 production by cobaloxime-based complexes. On the other hand, biology has widely employed the imidazole side chain from the histidine residue for anchoring metal cofactors, especially in hemoproteins.[118,119] Following this lead, Artero *et al.* have rationally inserted two different variants of cobaloxime motifs (hydrogen-bonded [Co(DH)$_2$] and difluoroboryl annulated [Co(DBF$_2$)$_2$]) into the heme-binding pocket of *apo-Sperm-whale* myoglobin (*Sw*Mb) (Fig. 14A). These synthetic metalloproteins displayed photocatalytic activity for HER, although at a considerably reduced efficiency (TON ~ 3–4, calculated *vs.* [catalyst] in the presence of [Ru(bpy)$_3^{2+}$]PS) compared to the corresponding free cobaloximes. This drop in the catalytic activity was attributed to the strained flexibility experienced by the histidine-ligated cobaloxime in the heme-binding cavity, which in turn terminated the competitive binuclear pathway for H_2 production (Fig. 14B).[120] In a follow-up study, they tuned the reactivity of the cobaloxime-bound biohybrids by altering the heme-binding pocket. For this purpose, the cobaloxime cores were installed in the heme-binding cavity of two strains of heme oxygenase proteins: rat heme oxygenase 1 (HO1) and *Corynebacterium diphteriae* heme oxygenase (HmuO). The resultant synthetic metalloproteins demonstrated an increase of ~3 times in the photocatalytic HER activity (TON ~ 6.3–15.3, calculated *vs.* [catalyst] in the presence of deazaflavin PS) compared to either free or SwMb-supported cobaloxime [Co(DH)$_2$].[121]

Kato and Yagi explored cyclodextrins (cyclic oligosaccharides of glucose) as an alternative for protein structures to induce a supramolecular effect on the reactivity of cobaloximes. For this purpose, they have designed a 1:1 adduct between the sulfonated-cobaloxime [Co(DH)$_2$(pyridine-4-sulfonate)Cl] and β- and γ-cyclodextrin *via* host–guest interaction (Fig. 15A). Among them, only the γ-cyclodextrin bound cobaloxime exhibited a ~10% increase in photocatalytic HER activity in the presence of

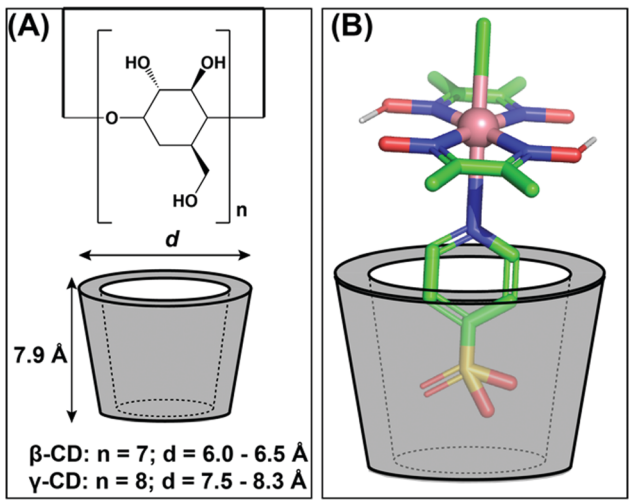

Fig. 15 (A) The basic structure of β- and γ-cyclodextrins (cyclic oligosaccharides of glucose) and their corresponding sizes. (B) The possible interaction between the sulfonate group from cobaloxime [Co(dmgH)$_2$-(pyridine-4-sulfonate)Cl] and the γ-cyclodextrin. These figures were redrawn from ref. 122.

Published on 05 June 2020. Downloaded on 1/24/2026 11:49:52 AM.

the Eosin-Y photosensitizer in aqueous solution (TON ~ 47, calculated *vs.* [catalyst] in the presence of Eosin-Y PS). The best-fitted insertion of the sulfonate group into the cyclodextrin cavity occurred in the case of γ-cyclodextrin, presumably due to the optimal size-matching. During the formation of this host–guest adduct, the core Co–N_4 motif of cobaloxime approached within the hydrogen-bonding distance with the hydroxyl groups present in the rim of the cyclodextrin (Fig. 15B). The dynamic proton exchange interaction between those groups possibly played a crucial role to induce the kinetic effect on the cobaloxime HER activity.[122]

Interestingly, the increment in the catalytic HER activity for these biohybrid constructs was either inconsequential (or even negative) compared to the free cobaloxime analogues. This observation suggested that the inclusion of cobaloxime inside the robust supramolecular structure may severely restrict the fluxionality of the cobaloxime motif to affect the overall reaction rate. A significant increase in the catalytic H_2 evolution was noticed only for a few constructs where the correctly oriented hydrogen-bonding interactions induced facile H^+ movement. The results from these earlier studies indicate that "*a minimally constrained cobaloxime motif containing a peripheral proton relay*" possibly holds the key for generating the second generation of enzyme-inspired cobaloxime-based H_2 production catalysts. Following this queue, a series of four cobaloxime complexes were created, where only the *para*-position of the axially coordinated pyridine ligand was altered, around an otherwise identical cobaloxime core [Co(DH)$_2$(pyridine-derivative)Cl]. Variable combinations of the secondary amine (–NH–), carboxylic acid group (–COOH), and phenolic (–Ph–OH) groups were utilized to fabricate one, two, and three-component proton relays in the cobaloxime periphery (Fig. 16).[99] The effect of the incorporation of the minimal (but essential) outer coordination sphere features was imminent as these cobaloxime derivatives were found to be active for electrocatalytic H_2 evolution in 100% aqueous solution. The three-component H^+-relay containing [ClCo(DH)$_2$-(pyridine–methylene–tyrosine)] recorded the fastest TOF for HER (~8830 s^{-1}, pH 7) among these complexes, which is a ~10-fold increase in the catalytic rate compared to the original [ClCo(DH)$_2$(pyridine)]. The catalytic rate for H_2 evolution for these complexes followed the following trend with varying pyridine substituents, tyrosine > tyramine ≈ phenylalanine > tyramine, to establish a direct connection between the extent of the outer coordination sphere feature and catalytic rate. This hypothesis was further supported by the two-dimensional Nuclear Overhauser effect spectroscopy (NOESY) NMR experiment, where a dynamic proton exchange among those peripheral basic groups, the oxime hydrogen-bonded network, and the solvent water molecules were observed. Typically, the cobaloxime motif becomes inactive for homogeneous H_2 production with increasing acidity of the solution (pH ≤ 5.0). The disruption of the oxime-derived hydrogen-bonding network, which acts as the protonation site during HER catalysis, is believed to be the prime reason for this behaviour. However, the outer coordination sphere functionalities present in the cobaloxime derivatives provides an alternate protonation spot, even in the acidic condition, to allow homogeneous H_2 production by those complexes even at pH 3–5. This particular aspect highlights that the incorporation of enzyme-inspired features can even impact the overall stability of the complexes. However, the effect of this distant protic groups is inferior in comparison to the closely lying oxime network, which is reflected by a contrasting change in the HER catalytic rate with a decrease in pH for all of those cobaloximes (Fig. 16).[99]

Next, the effect of such neighbouring basic groups on the cobaloxime motif was studied on the [Co(DH)$_2$(imidazole-derivative)Cl] platform, with an alternating axially ligated imidazole scaffold (Fig. 17).[68] The presence of multiple protic functionalities and their spatial orientation tunes the HER activity of these complexes. As expected, the natural amino acid histidine (which contains an imidazole side chain along with carboxylic acid and primary amine groups)-bound cobaloxime exhibited the highest kinetic rate (TOF ~ 4500 s^{-1}) for electrolytic H_2 production in a neutral aqueous solution. These complexes were probed even in the photocatalytic conditions to monitor the effect of the outer coordination sphere features

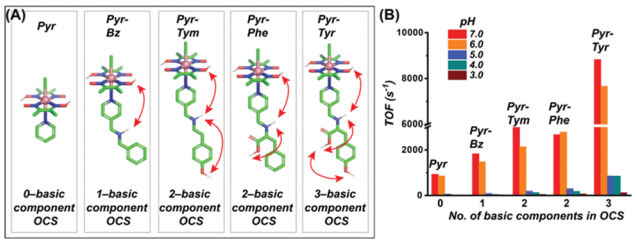

Fig. 16 (A) The basic structures of the [ClCo(dmgH)$_2$(pyridine-derivative)] complexes, along with the number of basic components present in their corresponding outer coordination sphere (OCS): (from left to right) only pyridine (Pyr), zero component; pyridine–methylene–benzylamine (Pyr–Bz), one component (–NH); pyridine–methylene–tyramine (Pyr–Tym), two components (–NH– and –Ph–OH); pyridine–methylene–phenylalanine (Pyr–Phe), two components (–NH– and –COOH); pyridine–methylene–tyrosine (Pyr–Tyr), three components (–NH–, –COOH, and –Ph–OH). (B) The experimentally tabulated electrocatalytic H_2 evolution reaction rate (TOF) variation for each complex in aqueous solution (pH 3.0–7.0). These figures were adapted from ref. 99.

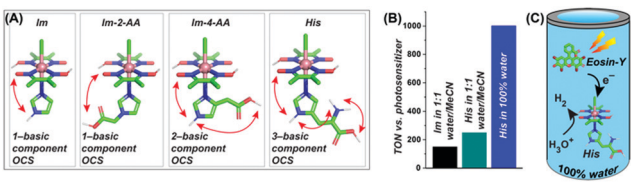

Fig. 17 (A) The basic structures of the [ClCo(DH)$_2$(imidazole-derivative)] complexes along with the number of basic components present in their corresponding outer coordination sphere (OCS): (from left to right) only imidazole (Im), one component (imidazole –NH–); imidazole-2-acetic acid (Im-2-AA), one component (–COOH); imidazole-4-acetic acid (Im-4-AA), two components (imidazole–NH– and –COOH); histidine (His), three components (imidazole–NH–, –COOH, and –NH_2). (B) The comparative TON (measured *vs.* photosensitizer) for photocatalytic H_2 evolution for Im (black bar) and His (cyan bar) in 1 : 1 water/acetonitrile, and His in 100% water (blue bar). (C) A schematic diagram of His activity in 100% water in the presence of Eosin-Y as a photosensitizer. These figures were adapted from ref. 68.

This journal is © The Royal Society of Chemistry 2020

Published on 05 June 2020. Downloaded on 1/24/2026 11:49:52 AM.

beyond the standard electrochemical settings. In the presence of the Eosin-Y dye, the overall photocatalytic H_2 production by $[Co(DH)_2(histidine)Cl]$ was enhanced by 1.7 times (TON ~ 250, calculated *vs.* [catalyst] in the presence of Eosin-Y PS), compared to the rudimentary $[Co(DH)_2(imidazole)Cl]$ in 1 : 1 water/acetonitrile media, to underline the impact of the additional protic groups appended from the imidazole. Again, the facile proton dynamics among these peripheral groups, along with the oxime and solvent water molecules, are believed to be the prime reason for this amplified HER performance. The presence of these enzyme-stimulated outer coordination sphere features even allowed us to obtain the first generation of fully water-soluble $[ClCo(DH)_2(imidazole\text{-}derivative)]$ complexes. This unique trait allowed us to achieve the first natural sunlight-irradiated photocatalytic H_2-producing cobaloxime complex that is active in an aerobic, neutral (pH 7.0) aqueous solution (TON ~ 1000, calculated *vs.* [catalyst] in the presence of Eosin-Y PS).[68] Hence, this enzyme-inspired complex represents an ideal candidate for investigating solar-driven H_2 production from water under the most practical circumstances.

Conclusions

Although cobaloxime was developed as a structural model for vitamin B12, it has recently gained more attention due to its catalytic properties for H_2 evolution reactions. The structural flexibility of this cobaloxime framework enabled the generation of a myriad of compounds with varying physiochemical electronic and solubility properties. The HER activity of the cobaloxime derivatives across a wide variety of conditions has established it as a diagnostic tool for optimizing photosensitizers for photocatalytic H_2 production. The display of better HER activity by the covalently-linked cobaloxime–photosensitizer adduct compared to independent segments established the significance of the directly coordinated photocatalytic assemblies for photo-driven H_2 production reactions. Later, the electrochemical investigation of cobaloximes provided insight into the intricacy of the structure–function relationship at the molecular level. Again, the versatility of the cobaloxime core shines as a critical element for probing its HER activity in both aqueous and non-aqueous solvent media. Despite all these advantages, the acid-instability of the primary coordination sphere-bound oxime motifs has narrowed the active HER catalytic space of cobaloximes to near-neutral conditions. Additionally, the poor H^+ movement around the core has limited the HER activity of cobaloximes to moderate compared to contemporary first-row transition metal-based catalysts. As a result, the cobaloxime-based HER research faced a lag period.

The architectural blueprint of metalloenzymes suggested that the inclusion of enzymatic hallmarks, such as an artificial proton relay, can influence the HER activity by cobaloxime. The simple yet robust nature of the cobaloxime core provided ample opportunity to either include cobaloxime into an already existing protein pocket, or rationally design a multi-component proton relay with precisely positioned peripheral functionalities around the core. This bio-mimetic catalyst design strategy has evolved a new genre of widely stable cobaloxime complexes that can photo-/electro-chemically produce H_2 at an unprecedented rate. Hence, the cobaloxime core is utilized as a model indicator for a broad spectrum of catalytic H_2 production functionalities, including optimizing the photocatalytic assembly, probing the electrocatalytic conditions, and exploring the effects of the peripheral enzyme-inspired features. In this review, we have covered the revival of the cobaloxime motif in the pursuit of a durable, efficient, and user-friendly H_2-producing catalyst, a key ingredient for the development of the H_2-based renewable energy infrastructure.

Conflicts of interest

There are no conflicts to declare.

Acknowledgements

The authors would like to thank the support provided by the Indian Institute of Technology Gandhinagar (IITGN) and Indian Institute of Technology Bombay (IITB). D. D. would like to thank the support of the DST-Inspire fellowship provided by the Department of Science and Technology (DST), India (DST/INSPIRE Fellowship/2017/IF170385). A. D. acknowledges the Ramanujan Fellowship (SB/S2/RJN-112/2015). P. M. would like to thank DST-SERB national post-doctoral fellowship (PDF/2018/000837).

Notes and references

1 D. C. Hodgkin, J. Kamper, M. Mackay, J. Pickworth, K. N. Trueblood and J. G. White, *Nature*, 1956, **178**, 64–66.
2 D. M. C. Hodgkin, J. Kamper, J. Lindsey, M. MacKay, J. Pickworth, J. H. Robertson, C. Brink-Shoemaker, J. G. White, R. J. Prosen and K. N. Trueblood, *Proc. R. Soc. London, Ser. A*, 1957, **242**, 228–263.
3 D. Lindsay and W. Kerr, *Nat. Chem.*, 2011, **3**, 494.
4 M. Giedyk, K. Goliszewska and D. Gryko, *Chem. Soc. Rev.*, 2015, **44**, 3391–3404.
5 G. N. Schrauzer, *Acc. Chem. Res.*, 1968, **1**, 97–103.
6 R. Dreos, S. Geremia, L. Randaccio and P. Siega, *PATAI'S Chemistry of Functional Groups*, American Cancer Society, 2010.
7 G. N. Schrauzer, G. W. Parshall and E. R. Wonchoba, *Inorganic Syntheses*, John Wiley & Sons, Ltd, 2007, pp. 61–70.
8 G. N. Schrauzer and J. Kohnle, *Chem. Ber.*, 1964, **97**, 3056–3064.
9 F. Wagner and K. Bernhauer, *Ann. N. Y. Acad. Sci.*, 1964, **112**, 580–589.
10 J. Hawecker, J. M. Lehn and R. Ziessel, *Nouv. J. Chim.*, 1983, **7**, 271.
11 A. Gerli and L. G. Marzilli, *Inorg. Chem.*, 1992, **31**, 1152–1160.
12 L. G. Marzilli, A. Gerli and A. M. Calafat, *Inorg. Chem.*, 1992, **31**, 4617–4627.
13 S. W. Ragsdale, P. A. Lindahl and E. Münck, *J. Biol. Chem.*, 1987, **262**, 14289–14297.
14 B. S. Tovrog, D. J. Kitko and R. S. Drago, *J. Am. Chem. Soc.*, 1976, **98**, 5144–5153.
15 A. Bakac and J. H. Espenson, *J. Am. Chem. Soc.*, 1984, **106**, 5197–5202.
16 P. Connolly and J. H. Espenson, *Inorg. Chem.*, 1986, **25**, 2684–2688.
17 M. Razavet, V. Artero and M. Fontecave, *Inorg. Chem.*, 2005, **44**, 4786–4795.
18 X. Hu, B. M. Cossairt, B. S. Brunschwig, N. S. Lewis and J. C. Peters, *Chem. Commun.*, 2005, 4723–4725.

Published on 05 June 2020. Downloaded on 1/24/2026 11:49:52 AM.

19 F. Lakadamyali, M. Kato, N. M. Muresan and E. Reisner, *Angew. Chem., Int. Ed.*, 2012, **51**, 9381–9384.
20 B. Ginovska-Pangovska, A. Dutta, M. L. Reback, J. C. Linehan and W. J. Shaw, *Acc. Chem. Res.*, 2014, **47**, 2621–2630.
21 A. Dutta, A. M. Appel and W. J. Shaw, *Nat. Rev. Chem.*, 2018, **2**, 244–252.
22 A. Panagiotopoulos, K. Ladomenou, D. Sun, V. Artero and A. G. Coutsolelos, *Dalton Trans.*, 2016, **45**, 6732–6738.
23 M. Yang, J. E. Yarnell, K. El Roz and F. N. Castellano, *ACS Appl. Energy Mater.*, 2020, **3**, 1842–1853.
24 X. Wang, S. Goeb, Z. Ji, N. A. Pogulaichenko and F. N. Castellano, *Inorg. Chem.*, 2011, **50**, 705–707.
25 E. Deponti and M. Natali, *Dalton Trans.*, 2016, **45**, 9136–9147.
26 J. L. Dempsey, B. S. Brunschwig, J. R. Winkler and H. B. Gray, *Acc. Chem. Res.*, 2009, **42**, 1995–2004.
27 R. Staehle, S. Losse, M. R. Filipovic, I. Ivanović-Burmazović, J. G. Vos and S. Rau, *ChemPlusChem*, 2014, **79**, 1614–1621.
28 L. Petermann, R. Staehle, M. Pfeifer, C. Reichardt, D. Sorsche, M. Wächtler, J. Popp, B. Dietzek and S. Rau, *Chem. – Eur. J.*, 2016, **22**, 8240–8253.
29 P. Du, K. Knowles and R. Eisenberg, *J. Am. Chem. Soc.*, 2008, **130**, 12576–12577.
30 B. Probst, C. Kolano, P. Hamm and R. Alberto, *Inorg. Chem.*, 2009, **48**, 1836–1843.
31 B. Probst, A. Rodenberg, M. Guttentag, P. Hamm and R. Alberto, *Inorg. Chem.*, 2010, **49**, 6453–6460.
32 A. Fihri, V. Artero, A. Pereira and M. Fontecave, *Dalton Trans.*, 2008, 5567–5569.
33 A. Fihri, V. Artero, M. Razavet, C. Baffert, W. Leibl and M. Fontecave, *Angew. Chem., Int. Ed.*, 2008, **47**, 564–567.
34 C. Li, M. Wang, J. Pan, P. Zhang, R. Zhang and L. Sun, *J. Organomet. Chem.*, 2009, **694**, 2814–2819.
35 K. L. Mulfort and D. M. Tiede, *J. Phys. Chem. B*, 2010, **114**, 14572–14581.
36 D. M. Cropek, A. Metz, A. M. Müller, H. B. Gray, T. Horne, D. C. Horton, O. Poluektov, D. M. Tiede, R. T. Weber, W. L. Jarrett, J. D. Phillips and A. A. Holder, *Dalton Trans.*, 2012, **41**, 13060–13073.
37 T. Auvray, R. Sahoo, D. Deschênes and G. S. Hanan, *Dalton Trans.*, 2019, **48**, 15136–15143.
38 M. Rupp, T. Auvray, E. Rousset, G. M. Mercier, V. Marvaud, D. G. Kurth and G. S. Hanan, *Inorg. Chem.*, 2019, **58**, 9127–9134.
39 C. Lentz, O. Schott, T. Auvray, G. Hanan and B. Elias, *Inorg. Chem.*, 2017, **56**, 10875–10881.
40 C. Lentz, O. Schott, T. Auvray, G. S. Hanan and B. Elias, *Dalton Trans.*, 2019, **48**, 15567–15576.
41 A. Mukherjee, O. Kokhan, J. Huang, J. Niklas, L. X. Chen, D. M. Tiede and K. L. Mulfort, *Phys. Chem. Chem. Phys.*, 2013, **15**, 21070–21076.
42 P. Du, J. Schneider, G. Luo, W. W. Brennessel and R. Eisenberg, *Inorg. Chem.*, 2009, **48**, 4952–4962.
43 P. Zhang, M. Wang, C. Li, X. Li, J. Dong and L. Sun, *Chem. Commun.*, 2009, 8806–8808.
44 P. Zhang, M. Wang, X. Li, H. Cui, J. Dong and L. Sun, *Sci. China: Chem.*, 2012, **55**, 1274–1282.
45 T. Lazarides, M. Delor, I. V. Sazanovich, T. M. McCormick, I. Georgakaki, G. Charalambidis, J. A. Weinstein and A. G. Coutsolelos, *Chem. Commun.*, 2013, **50**, 521–523.
46 M. Natali, R. Argazzi, C. Chiorboli, E. Iengo and F. Scandola, *Chem. – Eur. J.*, 2013, **19**, 9261–9271.
47 G. Landrou, A. A. Panagiotopoulos, K. Ladomenou and A. G. Coutsolelos, *J. Porphyrins phthalocyanines*, 2016, **20**, 534–541.
48 L. Mintrop, J. Windisch, C. Gotzmann, R. Alberto, B. Probst and P. Kurz, *J. Phys. Chem. B*, 2015, **119**, 13698–13706.
49 K. Peuntinger, T. Lazarides, D. Dafnomili, G. Charalambidis, G. Landrou, A. Kahnt, R. P. Sabatini, D. W. McCamant, D. T. Gryko, A. G. Coutsolelos and D. M. Guldi, *J. Phys. Chem. C*, 2013, **117**, 1647–1655.
50 J. Manono, P. A. Marzilli, F. R. Fronczek and L. G. Marzilli, *Inorg. Chem.*, 2009, **48**, 5626–5635.
51 R. S. Khnayzer, C. E. McCusker, B. S. Olaiya and F. N. Castellano, *J. Am. Chem. Soc.*, 2013, **135**, 14068–14070.
52 G. García-Herbosa, W. R. McNamara, W. W. Brennessel, J. V. Cuevas, S. Sur and R. Eisenberg, *Polyhedron*, 2013, **58**, 39–46.
53 W.-C. Xiao, Y.-W. Tao, Y. Zhao, J.-X. Luo and W.-Z. Lai, *Inorg. Chem. Commun.*, 2020, **113**, 107800.
54 P. Zhang, M. Wang, J. Dong, X. Li, F. Wang, L. Wu and L. Sun, *J. Phys. Chem. C*, 2010, **114**, 15868–15874.
55 T. M. McCormick, B. D. Calitree, A. Orchard, N. D. Kraut, F. V. Bright, M. R. Detty and R. Eisenberg, *J. Am. Chem. Soc.*, 2010, **132**, 15480–15483.
56 L. Gong, J. Wang, H. Li, L. Wang, J. Zhao and Z. Zhu, *Catal. Commun.*, 2011, **12**, 1099–1103.
57 T. Lazarides, T. McCormick, P. Du, G. Luo, B. Lindley and R. Eisenberg, *J. Am. Chem. Soc.*, 2009, **131**, 9192–9194.
58 E. Giannoudis, E. Benazzi, J. Karlsson, G. Copley, S. Panagiotakis, G. Landrou, P. Angaridis, V. Nikolaou, C. Matthaiaki, G. Charalambidis, E. A. Gibson and A. G. Coutsolelos, *Inorg. Chem.*, 2020, **59**, 1611–1621.
59 J. Dong, M. Wang, P. Zhang, S. Yang, J. Liu, X. Li and L. Sun, *J. Phys. Chem. C*, 2011, **115**, 15089–15096.
60 J. L. Dempsey, J. R. Winkler and H. B. Gray, *J. Am. Chem. Soc.*, 2010, **132**, 16774–16776.
61 D. D. Konieczna, H. Biller, M. Witte, W. G. Schmidt, A. Neuba and R. Wilhelm, *Tetrahedron*, 2018, **74**, 142–149.
62 Z.-Y. Wang, H. Rao, M.-F. Deng, Y.-T. Fan and H.-W. Hou, *Phys. Chem. Chem. Phys.*, 2013, **15**, 16665–16671.
63 H.-Q. Zheng, H. Rao, X.-Z. Hu, X.-H. Li, Y.-T. Fan and H.-W. Hou, *Sol. Energy*, 2014, **105**, 648–655.
64 G.-G. Luo, H. Lu, X.-L. Zhang, J.-C. Dai, J.-H. Wu and J.-J. Wu, *Phys. Chem. Chem. Phys.*, 2015, **17**, 9716–9729.
65 X. Li, G. Luo, K. Fang, J. Zhou, Q. Zhao and R. Wu, *Sci. Sin.: Chim.*, 2015, **45**, 843–854.
66 A. Xie, Z.-H. Pan, M. Yu, G.-G. Luo and D. Sun, *Chin. Chem. Lett.*, 2019, **30**, 225–228.
67 J. Wang, C. Li, Q. Zhou, W. Wang, Y. Hou, B. Zhang and X. Wang, *Dalton Trans.*, 2015, **44**, 17704–17711.
68 D. Dolui, S. Das, J. Bharti, S. Kumar, P. Kumar and A. Dutta, *Cell Rep. Phys. Sci.*, 2020, **1**, 100007.
69 X.-F. Liu, Y.-X. Zhang and J. Yan, *Transition Met. Chem.*, 2015, **40**, 305–311.
70 J. Bartelmess, W. W. Weare and R. D. Sommer, *Dalton Trans.*, 2013, **42**, 14883–14891.
71 J. Bartelmess, A. J. Francis, K. A. El Roz, F. N. Castellano, W. W. Weare and R. D. Sommer, *Inorg. Chem.*, 2014, **53**, 4527–4534.
72 G.-G. Luo, K. Fang, J.-H. Wu and J. Mo, *Chem. Commun.*, 2015, **51**, 12361–12364.
73 G.-G. Luo, K. Fang, J.-H. Wu, J.-C. Dai and Q.-H. Zhao, *Phys. Chem. Chem. Phys.*, 2014, **16**, 23884–23894.
74 J. C. Manton, C. Long, J. G. Vos and M. T. Pryce, *Phys. Chem. Chem. Phys.*, 2014, **16**, 5229–5236.
75 T. M. McCormick, Z. Han, D. J. Weinberg, W. W. Brennessel, P. L. Holland and R. Eisenberg, *Inorg. Chem.*, 2011, **50**, 10660–10666.
76 B. S. Veldkamp, W.-S. Han, S. M. Dyar, S. W. Eaton, M. A. Ratner and M. R. Wasielewski, *Energy Environ. Sci.*, 2013, **6**, 1917–1928.
77 A. Q. Mir, D. Dolui, S. Khandelwal, H. Bhatt, B. Kumari, S. Barman, S. Kanvah and A. Dutta, *JoVE*, 2019, e60231.
78 F. Lakadamyali and E. Reisner, *Chem. Commun.*, 2011, **47**, 1695–1697.
79 F. Li, K. Fan, B. Xu, E. Gabrielsson, Q. Daniel, L. Li and L. Sun, *J. Am. Chem. Soc.*, 2015, **137**, 9153–9159.
80 A. Morandeira, G. Boschloo, A. Hagfeldt and L. Hammarström, *J. Phys. Chem. B*, 2005, **109**, 19403–19410.
81 S. Lyu, J. Massin, M. Pavone, A. B. Muñoz-García, C. Labrugère, T. Toupance, M. Chavarot-Kerlidou, V. Artero and C. Olivier, *ACS Appl. Energy Mater.*, 2019, **2**, 4971–4980.
82 X.-W. Song, H.-M. Wen, C.-B. Ma, H.-H. Cui, H. Chen and C.-N. Chen, *RSC Adv.*, 2014, **4**, 18853–18861.
83 F. Niu, S. Shen, N. Zhang, J. Chen and L. Guo, *Appl. Catal., B*, 2016, **199**, 134–141.
84 T. Banerjee, F. Haase, G. Savasci, K. Gottschling, C. Ochsenfeld and B. V. Lotsch, *J. Am. Chem. Soc.*, 2017, **139**, 16228–16234.
85 J. Gu, Y. Yan, J. L. Young, K. X. Steirer, N. R. Neale and J. A. Turner, *Nat. Mater.*, 2016, **15**, 456–460.
86 N. R. Neale, N. Kopidakis, J. van de Lagemaat, M. Grätzel and A. J. Frank, *J. Phys. Chem. B*, 2005, **109**, 23183–23189.
87 A. Q. Mir, G. Joshi, P. Ghosh, S. Khandelwal, A. Kar, R. Hegde, S. Khatua and A. Dutta, *ACS Energy Lett.*, 2019, **4**, 2428–2435.
88 C. N. Valdez, J. L. Dempsey, B. S. Brunschwig, J. R. Winkler and H. B. Gray, *Proc. Natl. Acad. Sci. U. S. A.*, 2012, **109**, 15589–15593.

This journal is © The Royal Society of Chemistry 2020

Published on 05 June 2020. Downloaded on 1/24/2026 11:49:52 AM.

89 E. S. Rountree, B. D. McCarthy, T. T. Eisenhart and J. L. Dempsey, *Inorg. Chem.*, 2014, **53**, 9983–10002.
90 D. Dolui, S. Ghorai and A. Dutta, *Coord. Chem. Rev.*, 2020, **416**, 213335.
91 S. Cherdo, S. E. Ghachtouli, M. Sircoglou, F. Brisset, M. Orio and A. Aukauloo, *Chem. Commun.*, 2014, **50**, 13514–13516.
92 V. Artero and M. Fontecave, *Coord. Chem. Rev.*, 2005, **249**, 1518–1535.
93 J. A. S. Roberts and R. M. Bullock, *Inorg. Chem.*, 2013, **52**, 3823–3835.
94 X. Hu, B. S. Brunschwig and J. C. Peters, *J. Am. Chem. Soc.*, 2007, **129**, 8988–8998.
95 D. W. Wakerley and E. Reisner, *Phys. Chem. Chem. Phys.*, 2014, **16**, 5739–5746.
96 D. W. Wakerley, M. A. Gross and E. Reisner, *Chem. Commun.*, 2014, **50**, 15995–15998.
97 D. W. Wakerley and E. Reisner, *Energy Environ. Sci.*, 2015, **8**, 2283–2295.
98 X. Yin, C. Liu, S. Zhuo, Y. Xu and B. Zhang, *Dalton Trans.*, 2015, **44**, 1526–1529.
99 D. Dolui, S. Khandelwal, A. Shaik, D. Gaat, V. Thiruvenkatam and A. Dutta, *ACS Catal.*, 2019, **9**, 10115–10125.
100 N. M. Muresan, J. Willkomm, D. Mersch, Y. Vaynzof and E. Reisner, *Angew. Chem., Int. Ed.*, 2012, **51**, 12749–12753.
101 B. Reuillard, J. Warnan, J. J. Leung, D. W. Wakerley and E. Reisner, *Angew. Chem., Int. Ed.*, 2016, **55**, 3952–3957.
102 S. Donck, J. Fize, E. Gravel, E. Doris and V. Artero, *Chem. Commun.*, 2016, **52**, 11783–11786.
103 B. L. Wadsworth, A. M. Beiler, D. Khusnutdinova, S. I. Jacob and G. F. Moore, *ACS Catal.*, 2016, **6**, 8048–8057.
104 A. Krawicz, J. Yang, E. Anzenberg, J. Yano, I. D. Sharp and G. F. Moore, *J. Am. Chem. Soc.*, 2013, **135**, 11861–11868.
105 C. Tapia, E. Bellet-Amalric, D. Aldakov, F. Boudoire, K. Sivula, L. Cagnon and V. Artero, *Green Chem.*, 2020, **22**, 3141–3149.
106 S. Roy, Z. Huang, A. Bhunia, A. Castner, A. K. Gupta, X. Zou and S. Ott, *J. Am. Chem. Soc.*, 2019, **141**, 15942–15950.
107 I. Stassen, N. Burtch, A. Talin, P. Falcaro, M. Allendorf and R. Ameloot, *Chem. Soc. Rev.*, 2017, **46**, 3185–3241.
108 E. Mijangos, S. Roy, S. Pullen, R. Lomoth and S. Ott, *Dalton Trans.*, 2017, **46**, 4907–4911.
109 M. L. Helm, M. P. Stewart, R. M. Bullock, M. R. DuBois and D. L. DuBois, *Science*, 2011, **333**, 863–866.
110 W. Lubitz, H. Ogata, O. Rüdiger and E. Reijerse, *Chem. Rev.*, 2014, **114**, 4081–4148.
111 R. Cammack, M. Frey, R. Robson, M. Frey and R. Robson, *Hydrogen as a Fuel: Learning from Nature*, CRC Press, 2001.
112 T. R. Simmons, G. Berggren, M. Bacchi, M. Fontecave and V. Artero, *Coord. Chem. Rev.*, 2014, **270–271**, 127–150.
113 A. Dutta, D. L. DuBois, J. A. S. Roberts and W. J. Shaw, *Proc. Natl. Acad. Sci. U. S. A.*, 2014, **111**, 16286–16291.
114 L. M. Utschig, S. C. Silver, K. L. Mulfort and D. M. Tiede, *J. Am. Chem. Soc.*, 2011, **133**, 16334–16337.
115 L. M. Utschig, S. R. Soltau and D. M. Tiede, *Curr. Opin. Chem. Biol.*, 2015, **25**, 1–8.
116 S. R. Soltau, J. Niklas, P. D. Dahlberg, O. G. Poluektov, D. M. Tiede, K. L. Mulfort and L. M. Utschig, *Chem. Commun.*, 2015, **51**, 10628–10631.
117 S. R. Soltau, P. D. Dahlberg, J. Niklas, O. G. Poluektov, K. L. Mulfort and L. M. Utschig, *Chem. Sci.*, 2016, **7**, 7068–7078.
118 C. J. Reedy and B. R. Gibney, *Chem. Rev.*, 2004, **104**, 617–650.
119 T. L. Poulos, *Chem. Rev.*, 2014, **114**, 3919–3962.
120 M. Bacchi, G. Berggren, J. Niklas, E. Veinberg, M. W. Mara, M. L. Shelby, O. G. Poluektov, L. X. Chen, D. M. Tiede, C. Cavazza, M. J. Field, M. Fontecave and V. Artero, *Inorg. Chem.*, 2014, **53**, 8071–8082.
121 M. Bacchi, E. Veinberg, M. J. Field, J. Niklas, T. Matsui, D. M. Tiede, O. G. Poluektov, M. Ikeda-Saito, M. Fontecave and V. Artero, *ChemPlusChem*, 2016, **81**, 1083–1089.
122 M. Kato, K. Kon, J. Hirayama and I. Yagi, *New J. Chem.*, 2019, **43**, 10087–10092.